Termination, Isomerization, and Propagation Reactions during Ethene Polymerization Catalyzed by Cp_2Zr-R^+ and $Cp^*_2Zr-R^+$. An Experimental and Theoretical Investigation

Knut Thorshaug,[†] Jon Andreas Støvneng,[†] Erling Rytter,[*,†,‡] and Martin Ystenes[§]

Department of Industrial Chemistry, Norwegian University of Science and Technology (NTNU), N-7034 Trondheim, Norway, Statoil Research Centre, N-7005 Trondheim, Norway, and Department of Inorganic Chemistry, Norwegian University of Science and Technology (NTNU), N-7034 Trondheim, Norway

Received April 30, 1998; Revised Manuscript Received July 24, 1998

ABSTRACT: Ethene polymerization in toluene has been studied in the temperature range −7 to +97 °C and pressure range 0.28 to 9 bar, using two different L_2ZrCl_2/methylaluminoxane (MAO) catalyst systems. With bis(cyclopentadienyl)zirconium dichloride (Cp_2ZrCl_2, L = Cp), the average activity over 1 h increases with temperature between 10 and 97 °C. With bis(pentamethylcyclopentadienyl)zirconium dichloride ($Cp^*_2ZrCl_2$, L = Cp*), a maximum average activity over 1 h is observed at 45 °C. If propagation and deactivation effects are separated through kinetic modeling, the activity corresponding to chain propagation is found to increase in the whole temperature range for both catalysts. The molecular weight is higher with L = Cp* than with L = Cp below 80 °C. Above 80 °C, the opposite is observed. With L = Cp*, the molecular weight increases with increasing ethene pressure up to about 2 bar, where it levels off. With L = Cp, the molecular weight is independent of pressure between 0.28 and 9 bar. The ratio between vinyl and *trans*-vinylene unsaturation is approximately 6:1 with L = Cp and 1:1 with L = Cp*, both slightly increasing with increasing ethene pressure. As the temperature is increased, the relative vinyl content decreases with L = Cp and increases with L = Cp*. On the basis of density-functional calculations, we present a reaction scheme consistent with most of the experimental results. This reaction scheme, in which different agostic interactions play a crucial role, assumes a Cossee-like mechanism for chain propagation, chain termination via hydrogen transfer to a coordinated monomer (for both catalysts) or to the metal (for L = Cp*), and chain isomerization via partial hydrogen transfer to the metal, relative rotation of the olefin and the hydride, and reinsertion of the coordinated olefin. The calculated activation energy for propagation is 25−35 kJ/mol for L = Cp*, in fair agreement with the experimental value of 17 kJ/mol. For L = Cp, we calculate an activation energy of 10−20 kJ/mol, whereas the experimentally derived value is 61 kJ/mol. The poor agreement for L = Cp may indicate that the polymerization is influenced by the surrounding solvent and MAO. The calculated difference in activation energy between chain propagation and termination is larger for L = Cp* than for L = Cp, in qualitative agreement with the stronger temperature dependence of the molecular weight observed with L = Cp*. Chain isomerization is found to be easier, relative to termination, with L = Cp* than with L = Cp. This may account for the large amount of *trans*-vinylene unsaturation observed when $Cp^*_2ZrCl_2$ is used as catalyst.

1. Introduction

Metallocene catalysts have attracted considerable interest over the last years, due to their excellent properties in polymerizing α-olefins like ethene and propene. In particular, they are characterized by their high activity and the ability to produce a polymer with high molecular weight and a narrow molecular-weight distribution. A number of review articles have appeared lately,[1−5] reflecting the intensity of research in this field.

The large amount of experimental and theoretical work on metallocene catalysis has led to substantial insight into the reaction mechanisms that influence the polymerization process and the polymer properties. For chain propagation, most of the studies reported[6−10] support a Cossee-like mechanism.[11] Studies on chain termination[12−25] suggest that it occurs by elimination of a β-hydrogen, by transfer to either the metal or to a coordinated monomer. Recent experimental results on ethene polymerization catalyzed by Cp_2ZrCl_2/MAO [Cp = C_5H_5, cyclopentadienyl; MAO = methylaluminoxane] suggest that transfer to monomer dominates in this system.[19] This conclusion is supported by others,[15,25] but different results have also been reported.[20] Isomerization has been identified as an important mechanism in order to explain stereoirregularities and misinsertions during polymerization of propene, e.g., 1−3 insertion.[26−31] Theoretical calculations[32] have verified the possibility of a proposed isomerization path that involves a relative rotation of the alkyl chain and the ligand framework.[4,26] Recently, isomerization was suggested to occur also during polymerization of ethene with Cp_2ZrCl_2/MAO.[19]

In an attempt to address how the metallocene ligands affect the mechanisms of propagation, termination, and isomerization, we have performed an extensive comparative study of the two catalysts L_2ZrCl_2, with L = Cp and L = Cp* [Cp* = Me_5C_5, pentamethylcyclopentadienyl]. The aim of this work is to quantify experimentally the differences between the two systems and to compare these results with differences revealed by quantum chemical modeling. A close correlation between theoretical results and results of carefully performed experimental studies will constitute a strong foundation for explanations of the processes involved.

* Corresponding author. E-mail: erling.rytter@statoil.com
† Department of Industrial Chemistry.
‡ Statoil Research Centre.
§ Department of Inorganic Chemistry.

10.1021/ma980694k CCC: $15.00
Published on Web 09/30/1998

Scheme 1. Subsequent Insertions to γ-Agostic Structures

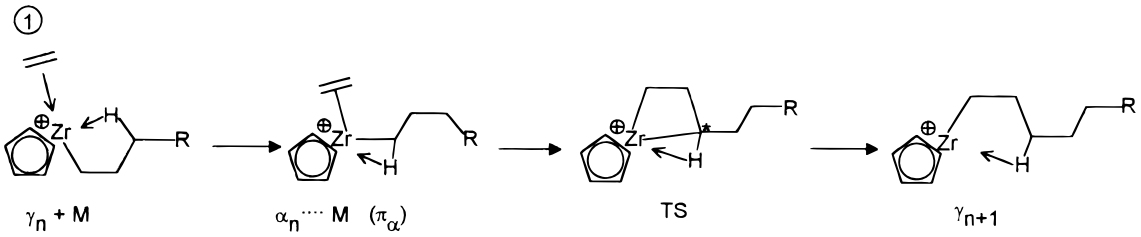

Scheme 2. Rotation between γ- and β-Agostic Conformation

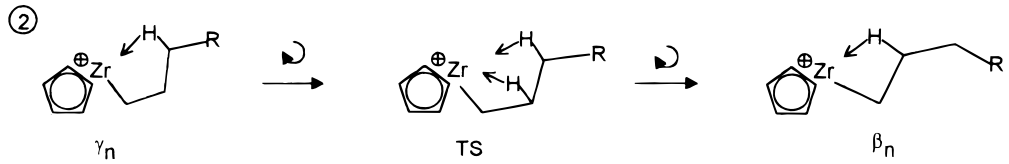

Scheme 3. Frontside Insertion to β-Agostic Structure

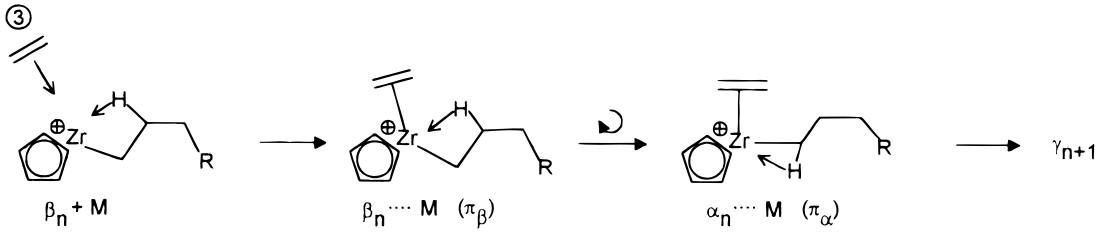

Scheme 4. Backside Insertion to β-Agostic Structure

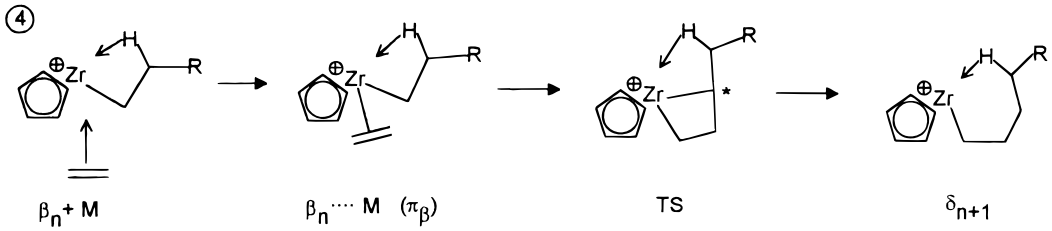

Results in the literature[33−35] indicate that the catalyst with L = Cp* is less active than with L = Cp during ethene polymerization, and the molecular weight of the polyethene produced has been reported to be both higher[34] and lower[35] with L = Cp* than with L = Cp. Further, since chain isomerization is believed to proceed via a rotation reaction (see Scheme 7 below), one might expect this process to be hindered by the bulky and sterically demanding Cp* ligands. As will be discussed later, statements like these need to be elaborated in more detail.

Due to the high complexity of these systems, a number of different reaction mechanisms are conceivable. Thus, it is not possible to explore all possibilities with reaction-pathway modeling. We have selected a set of mechanisms that we believe is necessary to account for the experimental observations. With density-functional calculations, we have tried to assess the relative importance of the different mechanisms for the L = Cp and L = Cp* catalysts. The key reaction steps involved are as follows:

Chain *propagation* proceeds mainly according to a Cossee-like mechanism, with insertion to a γ-agostic structure (Scheme 1). The insertion goes via an α-agostic π-complex and a four-center transition state (TS) to a product which is again γ-agostic. The alkyl chain may rotate from a γ-agostic to a β-agostic conformation[9,17] (Scheme 2). Monomer approach to a β-agostic structure may also result in chain propagation.[15] The alternative mechanisms then are frontside insertion via a rotation from a β-agostic to an α-agostic π-complex (Scheme 3) or backside insertion to a δ-agostic product (Scheme 4).

Chain *termination* typically starts from a β-agostic structure. The termination step may then take place via transfer of a β-hydrogen to a coordinated monomer (Scheme 5) or to the metal center (Scheme 6, β-hydride elimination).

Chain *isomerization* starts with partial transfer of H_β to the metal, i.e., partial β-hydride elimination, followed by a relative rotation of the coordinated olefin and the metallocene hydride. Transfer of the hydrogen back to the olefin completes the isomerization and results in a structure with one primary and one secondary β-carbon (Scheme 7).

Based on the quantum-mechanically derived energetics of the various reaction steps with L = Cp and L = Cp*, we will argue that these mechanisms are indeed relevant to the ethene polymerization experiments.

The rest of the paper is organized as follows. In the next sections we include some experimental (section 2) and computational (section 3) details. In sections 4 and 5, we present our experimental and theoretical results. Conclusions, based on a comparison between experiment and theory, are drawn in section 6. Additional figures and tables are available as Supporting Information.

Scheme 5. Termination by Transfer of H_β to Coordinated Monomer

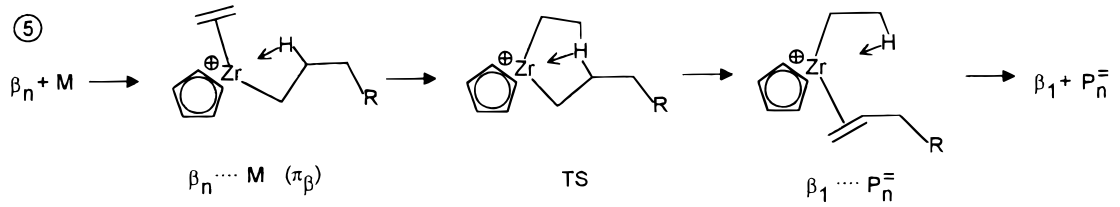

Scheme 6. Termination by Transfer of H_β to the Metal

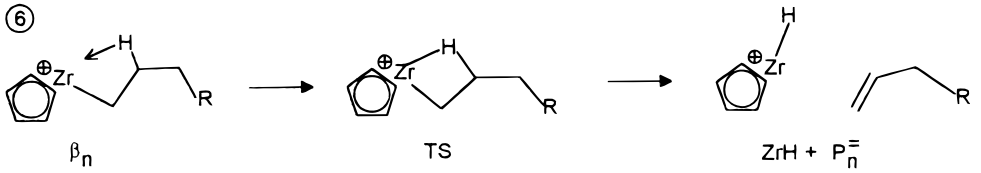

Scheme 7. Reaction Path for Alkyl Chain Isomerization

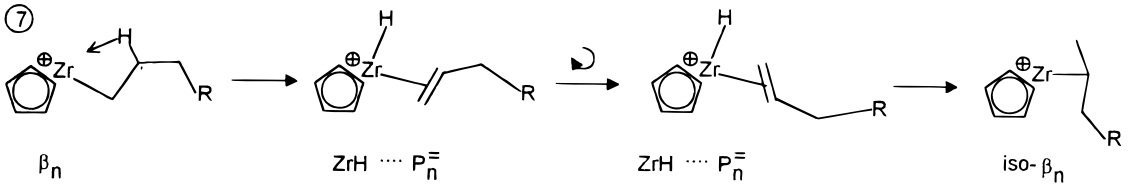

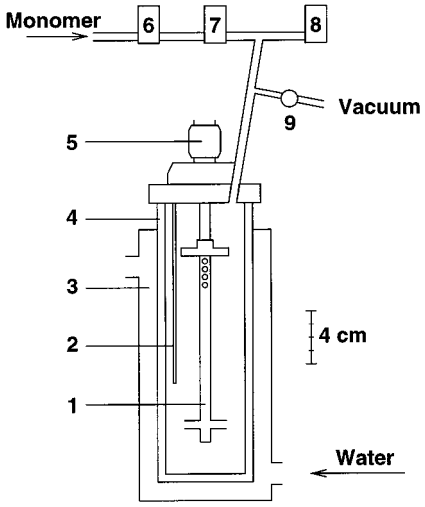

Figure 1. Sketch of the polymerization reactor and the connected electronic units: (1) stirrer, (2) Pt−100 thermoelement, (3) water jacket, (4) reactor, (5) connection to motor for stirring (Motor not shown for clarity), (6) mass flow meter, (7) pressure controller, (8) pressure meter, (9) valve for evacuation.

2. Experimental details

2.1. Apparatus. A sketch of the experimental setup is given in Figure 1. The pressure was kept constant within 0.05 bar by an electronic pressure controller. Monomer flow, pressure, and reactor temperature were logged at a rate of 12 Hz and an average per second was written to a computer file.

2.2. Chemicals. Bis(cyclopentadienyl)zirconium dichloride (Cp_2ZrCl_2) and bis(pentamethylcyclopentadienyl)zirconium dichloride ($Cp^*_2ZrCl_2$) from Boulder Scientific Co., 10 wt % methylaluminoxane (4.6% Al) in toluene from Albemarle S.A., nitrogen (99.999%) from Hydro Gas, and ethene (polymerization grade) from Borealis were all used as received. Toluene (p.a.) from Prolabo was refluxed over sodium/benzophenone and distilled under a nitrogen atmosphere before use. Standard glovebox and Schlenk techniques were used during all manipulations.

2.3. Polymerization. Before use, the reactor was kept at 150 °C for at least 2 h. Catalyst was dissolved in toluene (100 mL). The reactor was mounted, repeatedly evacuated ($P \leq 0.1$ mbar), and purged with, first, nitrogen and, finally, ethene. The desired reactor temperature was set, toluene (200 mL) was introduced to the reactor, and the stirring rate was set (1850 rpm). After 30 min MAO (1 mL) was injected and after an additional 7 min catalyst dissolved in toluene was injected to give [Al]/[Zr] = 2200. The reaction was stopped by closing the monomer feed, and the product was poured into a mixture of methanol (300 mL) and concentrated hydrochloric acid (30 mL). After filtration, the polymer was washed with methanol and dried. The polymer was stored without additives in a refrigerator.

2.4. Polymer Characterization. Fourier transform infrared (FTIR) spectroscopy, gel permeation chromatography (GPC), and differential scanning calorimetry (DSC) were performed according to previously reported procedures.[19]

3. Computational Details

3.1. Density-Functional Calculations. All calculations were carried out using the density-functional program DMol (Versions 2.36, 3.00, and 4.00) provided by MSI (formerly Biosym).[36] A double-numeric basis set including polarization functions was used (DNP option in DMol), with the 1s carbon and 1s to 3d zirconium orbitals assigned to a frozen core. The potential was evaluated at the level of the local-density approximation, using the local correlation functional of Lee *et al.*[37] Geometries were optimized with approximate gradient corrections included. Gradient corrections to the energy were based on the functionals proposed by Becke (for exchange)[38] and Lee *et al.* (for correlation).[37] Insertion of ethene into $Cp_2ZrCH_3^+$ was also studied with gradient corrections included in the self-consistent potential. Basically, the whole energy curve was shifted downward by about 8 kJ/mol, leaving the insertion energy barrier almost unaffected.

We have performed a large number of linear-transit (LT) calculations in an attempt to explore the energetics along alternative reaction pathways. In LT calculations, an LT reaction coordinate (a bond distance, bond angle, or dihedral angle) is held fixed and changed stepwise, whereas all other degrees of freedom are

Table 1. Experimentally Obtained Activity and Polymer Characteristics from Polymerization of Ethene by $Cp^*_2ZrCl_2$/MAO ([Al]/[Zr] = 2200) in Toluene at T = 80 °C

run	P_{Ethene} (bar)	C_{Ethene} (mol/L)	$10^{-3}M_n$ (IR)	$10^{-3}M_n$ (GPC)	M_w/M_n (GPC)	*trans*-vinylene/vinyl[a]	T_m (°C)	yield (g)	av activity (tonne of PE/mol of Zr·h)
1	0.28	0.0208						0.31	366
2	0.30	0.0222	42.4	5.2	5.2	0.190/0.140	130.5[b]	0.32	378
3	0.33	0.0243						0.19	225
4	0.37	0.0271						0.20	236
5	0.50	0.0362						0.19	225
6	0.59	0.0426	77.3	7.4	4.0	0.093/0.088	135.1	0.59	704
7	0.75	0.0538						1.33	1567
8	0.81	0.0581	29.7	13.0	3.8	0.267/0.205	132.9	0.99	861
9	0.98	0.0700						1.54	1444
10	0.99	0.0707				0.142/0.120		0.64	758
11	1.00	0.0714	50.7	22.0	4.4	0.180/0.097	133.5	0.33	392
12	1.20	0.0855	37.3	19.0	4.4	0.194/0.182	133.9	2.20	2667
13	1.59	0.1130						3.31	3954
14	1.76	0.1250						0.22	233
15	2.02	0.1434	57.6	47.0	3.2	0.129/0.114	134.9	1.86	2224
16	2.50	0.1773	48.6	22.0	6.2	0.130/0.159	133.3	5.54	6720
17	2.53	0.1795	46.9	22.0	5.8	0.132/0.168	134.3	5.55	6720
18	2.59	0.1837	40.9			0.152/0.191	135.1	5.23	6247
19	2.83	0.2007						6.50	7740
20	3.02	0.2141	54.7			0.121/0.136		6.10	7394
21	3.60	0.2553						4.32	5160
22	3.99	0.2829	219	30	7	0.037/0.027		4.20	5004
23	4.01	0.2844						7.65	9101
24	4.01	0.2844	54.8	30	5.4	0.110/0.146		7.26	8797
25	4.02	0.2851	57.5	35	4.4	0.109/0.134	134.3	8.00	9691
26	4.81	0.3412	56.0	22	6.3	0.099/0.151	134.4	9.20	10946
27	4.99	0.3540						9.96	12064
28	7.61	0.5411	59.4	23	10	0.111/0.125	136.3	10.64	12702

[a] Per 1000 C atoms. [b] Only 1 mg was used due to low yield. FTIR and GPC were given higher priority.

Scheme 8. Kinetic Model

$$L_2ZrCl_2 + MAO \xrightarrow{k0} L_2ZrCH_3^+ + \text{"MAO}^-\text{"} \quad (0)$$

$$L_2ZrCH_3^+ + C_2H_4 \xrightarrow{k1} P_1 \quad (1)$$

$$P_n + C_2H_4 \xrightarrow{k2} P_{n+1} \quad (2)$$

$$P_n \xrightarrow{k3} L_n \quad (3)$$

$$L_n + C_2H_4 \xrightarrow{k4} P_{n+1} \quad (4)$$

$$L_n \xrightarrow{k5} D \quad (5)$$

completely relaxed. In order to prove that energy maxima and minima along the LT curves are true transition states and true minima, respectively, one must evaluate the vibrational frequency spectrum for each stationary geometry and check for the occurrence of one and zero imaginary eigenvalues, respectively. Such calculations are extremely time consuming and were only done for a few reaction pathways, all with Cp as ligands. However, the experience from those calculations seems to give strong evidence that all stationary points found on the LT curves are at least close to true minima or saddle points of the potential-energy surface. Also note that calculated energy differences refer to electronic energies. Enthalpies and Gibbs free energies would require complete frequency calculations, which are at present out of reach.[39]

3.2. Kinetic Modeling. During a (semibatch) polymerization experiment, the activity is not constant. Typically, its time profile is characterized by periods of activation and deactivation, and a constant asymptotic value is usually approached after several minutes of polymerization.

In an attempt to extract a rate constant for chain propagation where deactivation is excluded from the activity data, we assume that the kinetics may be described with the simple model given in Scheme 8.[40]

This model accounts for the following reaction mechanisms:

- alkylation and ionization of the zirconocene dichloride in a reaction with MAO, i.e., activation of the catalyst (eq 0)
- insertion of the first monomer, i.e., initiation of the chain propagation (eq 1)
- insertion of subsequent monomers, i.e., the typical propagation step (eq 2).
- formation of latent sites, i.e., nonpermanent deactivation of active sites (eq 3)
- reactivation of latent sites (eq 4)
- permanent deactivation (eq 5)

With as many as six fitting parameters, the model in Scheme 8 overfits the activity time profiles. This problem has been reduced by using an even simpler model based on eqs 1−4 only. The value obtained for the propagation rate constant k_2 is very little affected by such a model reduction.

4. Experimental Results

4.1. Catalytic Activity. Data given in Tables 1 and 2 show the effect of pressure and reaction temperature, respectively, on the polymerization kinetics and the polymer properties. A graphical presentation of the temperature effect on the average catalytic activity over 1 h is shown in Figure 2. Figure 3 is an Arrhenius plot of the corrected activity based on the propagation rate constant k_2 derived with the kinetic model in Scheme 8. In Figure 4, examples of the monomer consumption rate as function of reaction time at P_{Ethene} = 1.0 bar and T = 56 °C and T = 80 °C are presented.

Table 2. Experimentally Obtained Activity and Polymer Characteristics from Polymerization of Ethene by L_2ZrCl_2/MAO (L = Cp, Cp*; [Al]/[Zr] = 2200) in Toluene at P_{Ethene} = 1 bar

										tonne of PE/mol of Zr·h·C_{Ethene}	
run	L	T_p (°C)	C_{Ethene} (mol/L)	$10^{-3}M_n$ (IR)	$10^{-3}M_n$ (GPC)	M_w/M_n	trans-vinylene/vinyl[a]	T_m (°C)	yield (g)	av activity	corrected activity
29	Cp	10	0.2319						*b*		5
30	Cp	10	0.2319						1.13	6	6
31	Cp	30	0.1250						1.17	17	10
32	Cp	56	0.0905	114			0.0068/0.0091	137.0	6.96	97	104
33	Cp	61	0.0867	89.4			0.0103/0.1202	136.9	10.01	146	299
34	Cp	71	0.0769	71.3			0.0172/0.1792	136.5	9.72	160	250
35	Cp	73	0.0728					132.9	18.37	319	882
36	Cp	82	0.0686	50.5			0.0329/0.2560	135.4	20.60	380	759
37	Cp	93	0.0598	36.7			0.0670/0.4478	133.0	19.72	417	1342
38	Cp	97	0.0578	26.3			0.0847/0.5062	133.5	20.25	443	1548
39	Cp*	−7	0.2312					135.5	1.13	6	68
40	Cp*	22	0.1421					135.5	9.99	84	171
41	Cp*	33	0.1330					136.0	9.25	83	353
42	Cp*	42	0.1114		150	2.5		135.7	15.28	176	500
43	Cp*	51	0.0949					135.9	12.51	159	456
44	Cp*	51	0.0949	603	23	4.3	0.0164/0.0068	136.9	12.64	157	475
45	Cp*	56	0.0888	399	70	3.1	0.0244/0.0107	135.2	9.65	130	490
46	Cp*	60	0.0863		53	3.4		134.7	8.29	115	539
47	Cp*	60	0.0863	219	134	2.9	0.0359/0.0281	136.0	6.30	87	
48	Cp*	70	0.0773	119	25	3.8	0.0642/0.0530	133.7	4.37	67	642
49	Cp*	80	0.0700	71.7	26	4.0	0.1058/0.0895	133.5	0.83	14	539
50	Cp*	90	0.0685	16.8	9	5.1	0.4122/0.4197	131.9	0.66	11	451

[a] Per 1000 C atoms. [b] Stopped after short time, only first part of the curve was used for kinetic modeling.

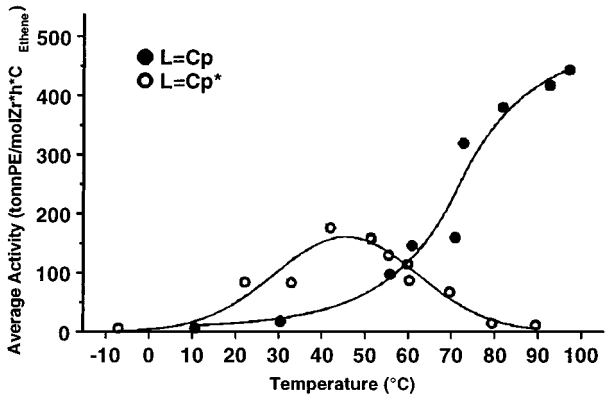

Figure 2. Average polymerization activity over 1 h as a function of reaction temperature with L_2ZrCl_2/MAO in toluene and P_{Ethene} = 1.0 bar (L = Cp, Cp*).

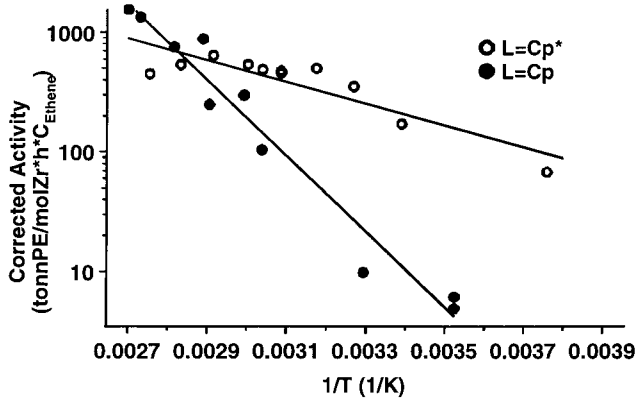

Figure 3. Arrhenius plots of the modeled corrected activity for the polymerization of ethene with L_2ZrCl_2/MAO in toluene and P_{Ethene} = 1.0 bar (L = Cp, Cp*).

The catalytic activity was found to increase with increasing monomer pressure, as seen from the data in Table 1. By plotting ln(average activity) versus ln(monomer pressure), the reaction order was found to be $\alpha = 1.4$ for L = Cp*. From the data given by Chien and Wang,[20] we found $\alpha = 0.99$ for L = Cp. The reaction order is often found to be in the range $1 \leq \alpha \leq 2$, and a thorough discussion has been offered by Brintzinger *et al.*[4]

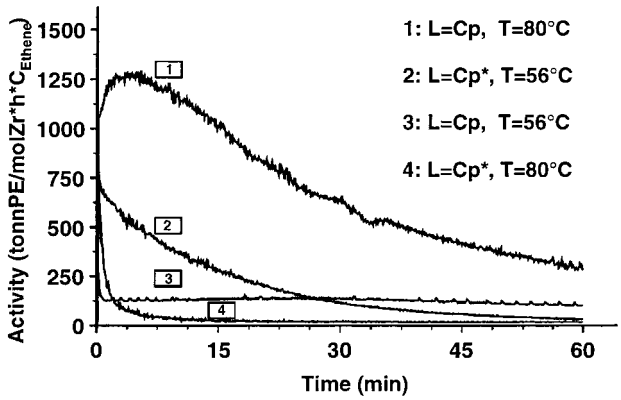

Figure 4. Reaction rate as a function of time at T = 56 and 80 °C with L_2ZrCl_2/MAO in toluene and P_{Ethene} = 1.0 bar (L = Cp, Cp*).

The average activity over 1 h behaves very differently with respect to reaction temperature for the two catalysts, as seen from Figure 2. In the case of L = Cp, the average activity increases steadily in the whole temperature range, whereas for L = Cp*, the average activity over 1 h passes through a maximum at approximately 45 °C. From Figure 4, it is seen that the catalytic activity is time dependent and this influences heavily on the position of the maximum average activity versus temperature. If the average is taken over a time interval from 0 to t minutes, with $0 < t < 60$, the maximum is shifted toward higher temperatures when t is decreased. In the case of L = Cp*, we observe a shift in the temperature of maximum average activity, as shown in Figure 5. This illustrates that the position of maximum average activity versus polymerization temperature is not only dictated by the experimental conditions, but also by the treatment of the data with respect to time. Note that the curve in Figure 5 appears

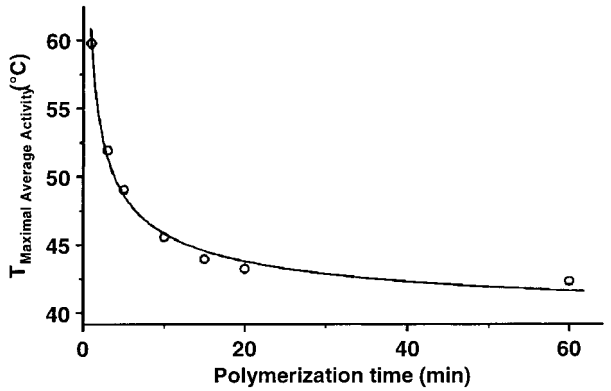

Figure 5. Temperature of maximum average activity as a function of polymerization time with $Cp^*_2ZrCl_2$/MAO in toluene and $P_{Ethene} = 1.0$ bar.

to approach the *y*-axis asymptotically as the polymerization time *t* approaches zero. This implies that the initial activity is not influenced by deactivation and hence simply increases with increasing temperature.

In an attempt to obtain a corrected activity corresponding to an intrinsic propagation rate, kinetic modeling was performed according to the model described in section 3.2. The observed reaction rate is then separated into terms that express the rate of the different reactions according to Scheme 8, i.e., activation, propagation, and deactivation. The corrected activity data are listed in Table 2. They follow an Arrhenius relationship, as shown in Figure 3. On the basis of the corrected reaction rates, we obtain activation energies for propagation of 61 ±4 kJ/mol with L = Cp and 17 ± 3 kJ/mol with L = Cp*. On the basis of the average activity over 1 h, we find the activation energies to be 46 ± 3 kJ/mol for L = Cp and 43 ± 5 kJ/mol for L = Cp*, the latter based on the data between −7 and +51 °C only.

From data in the literature for L = Cp, we have calculated activation energies E_a based on average activities. We have used kg of PE/mol of Zr·h·C_{Ethene} as units throughout and find E_a values of 28,[41] 37−40[42] and 58 kJ/mol.[43] From the average activity data given on polymerization of ethene by Cp_2ZrCl_2 in *n*-heptane,[44] we calculate an activation energy of 34 kJ/mol. These values are in reasonable agreement with our value of 46 kJ/mol. The differences observed might be due to different experimental conditions ([Al]/[Zr] ratio, type of solvent, etc.). In fact, it could be taken as an indication that the observed activation energy is influenced by experimental conditions and is not simply a measure of the energy barrier of the intrinsic propagation step. This can also explain the large discrepancy between the experimental and theoretical value (see section 5.1 below) in the case of L = Cp.

Since the activity is time dependent, activation energies based on average activities will, in general, deviate from the values obtained by kinetic modeling. Various reaction schemes may be considered in order to describe the observed kinetics, and other schemes may be more realistic than the one chosen here in their description of the reactions that occur. However, the propagation rate constant k_2, from which the corrected activity is derived, does not change much when different kinetic models are used.

On the basis of the data in Figure 2, this work shows that under the given experimental conditions, the average activity of L = Cp is larger than that of L = Cp* at $T \geq 60$ °C. At $T < 60$ °C, the situation is reversed. The activities obtained by kinetic modeling indicate that the L = Cp* catalyst is more active than the one with L = Cp up to about 80 °C. In earlier reports,[33−35] it is stated that the catalytic activity toward ethene polymerization is larger with L = Cp than with L = Cp*. The conclusions based on experiments performed at a single temperature of 70[33] and 80 °C[35] compare well with our average activity data for the same temperatures. Naturally, with measurements at a single temperature only, the crossover at about 60 °C was not observed. Kaminsky *et al.*[34] polymerized at two temperatures, 20 and 70 °C, and only average activities were considered. We have shown the importance of several measurements over a large temperature range and a careful treatment of the data with respect to time, together with kinetic modeling. As far as we know, these improvements in data collection and analysis extend beyond what has been previously reported. We believe this is the reason for the different conclusions reached in earlier reports and in the present work.

Various results can be found in the literature on the catalytic activity with L = Cp. In one paper, the average activity was reported to increase in the range 0−30 °C and to remain constant in the range 30−80 °C.[41] In another, it was claimed that the activity increases steadily from 25 to 70 °C.[42] Finally, the catalytic activity has also been claimed to increase in the range 30−60 °C and to decrease in the interval 70−80 °C.[43] Before comparing with our data, the results referred to above were corrected for monomer concentration at different temperatures. Then, the average activity increases steadily over the whole temperature range in the first two reports,[41,42] as observed in the present work. The data of Peng and Xiao[43] still showed a maximum value between 70 and 80 °C. In *n*-heptane, the behavior is different.[44] A moderate increase in catalytic activity was observed in the temperature range −20 to +70 °C, but from 70 to 80 °C the activity increased dramatically. This was ascribed to better solubility of polyethene at elevated temperatures. In our work, the polyethene produced at 93 °C appeared to be completely dissolved in toluene. By visual inspection, the product was a clear see-through liquid with a viscosity larger than that in pure toluene. In contrast, at 80 °C, a white polymer precipitate was formed during the reaction. In spite of this difference in solubility of the polymer, we could not detect variations in activity beyond the expected Arrhenius behavior. This indicates that the polymerization rate is not limited by diffusion in the polymer particles. This is supported by a constant $E_a(1/T)$ over the whole temperature range, and estimates of the Thiele modulus and Weisz−Prater values are both below 1.[45] No data on temperature effects on polymerization of ethene with L = Cp* could be found in the literature.

It is interesting to note that although the activities of L = Cp and L = Cp* are very different with respect to time, as seen from Figure 4, they can both be described with the kinetic model in Scheme 8. In order to describe the reaction profiles, deactivation reactions are of utmost importance. In Figure 6, the activity after repeated additions of catalyst (L = Cp*) and MAO is shown. The metallocene and MAO were mixed at $t = 0$ and kept in a separate Schlenk-bulb at $T = 29$ °C. Every 30 min identical mixtures of metallocene and MAO in toluene ([Al]/[Zr] = 2200) were added. Figure

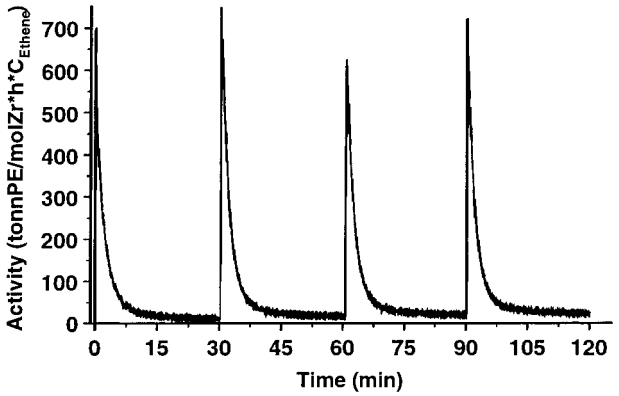

Figure 6. Reaction rate as a function of time with repeated injections of $Cp^*_2ZrCl_2$/MAO at $T = 80$ °C and $P_{Ethene} = 1.0$ bar.

6 clearly shows that the catalyst does not deactivate when there is no monomer or polymer present. Thus, the deactivation must involve the metallocene−MAO−growing chain complex and possibly also the monomer. Further, Figure 6 shows that the maximum reactivity is reached instantaneously with the same peak value regardless of the contact time of the metallocene and MAO prior to injection. As might be expected, the steady-state value increases when more metallocene-MAO mixture is added to the reactor.

Separate experiments with L = Cp, in which the [Al]/[Zr] ratio is increased, give a moderately higher reaction rate, in accordance with the literature.[41]

4.2. Chain Termination and Isomerization. As listed in Table 1 and shown in Figure 7A, for L = Cp* the number average molecular weight M_n increases with monomer pressure at low ethene pressures. At higher pressures, M_n seems to be pressure independent.[46] For L = Cp, we recently reported the molecular weight to be pressure independent at $T = 50$ °C. This is shown in Figure 7B. M_n is proportional to the ratio between the kinetic constants of propagation and termination, as expressed in eq 6.

$$M_n = 0.028 \frac{k_p[C_2H_4]}{k_t^0 + k_{t,M}[C_2H_4]} \quad \text{(kg/mol)} \qquad (6)$$

Here, k_p is the rate constant for propagation. Termination reactions independent of monomer concentration are represented by k_t^0 and include β-H transfer to Zr and chain transfer to Al in MAO. Termination via β-H transfer to a coordinated monomer occurs at a rate of $k_{t,M}$. The monomer concentration $[C_2H_4]$ is in the liquid phase.

For L = Cp*, our data are consistent with a reaction scheme where termination occurs both via β-H transfer to a coordinated monomer and via monomer independent mechanisms. A fit of eq 6 to the experimental GPC and FTIR data is shown in Figure 7A, and the corresponding kinetic constant ratios are given in Table 3. In order to describe the data, both termination via transfer of H_β to monomer and monomer independent termination must be taken into account. For L = Cp, the data in Figure 7B indicate that M_n is independent of monomer concentration over the whole range studied. Thus, we concluded that termination occurs preferably by β-H transfer to a coordinated monomer.[19] The same conclusion has been reached by D'Agnillo *et al.*[25] and Lohrenz *et al.*[15]

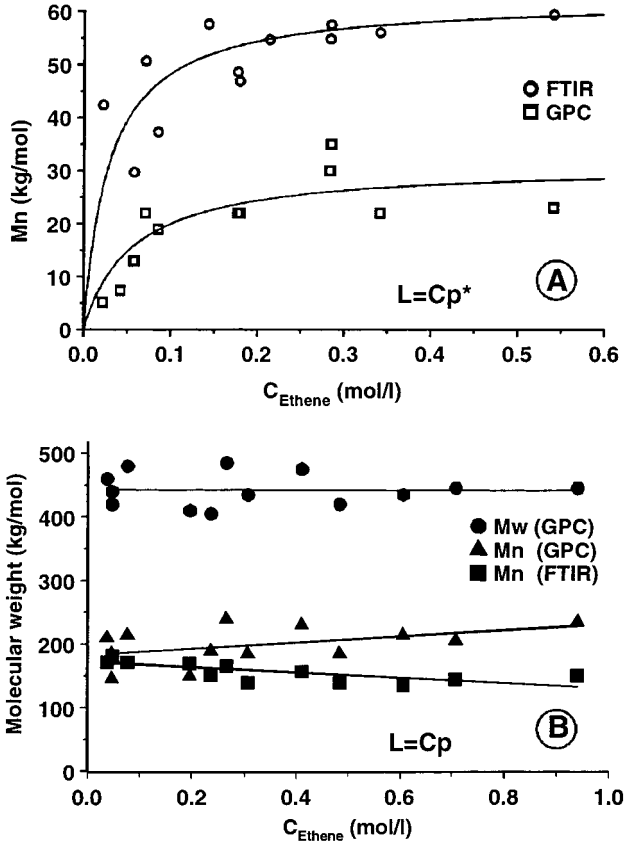

Figure 7. Relative average molecular weight as a function of monomer concentration: (A) L = Cp*, $T = 80$ °C; (B) L = Cp, $T = 50$ °C. Data for L = Cp from ref 19.

Table 3. Experimentally Determined Activation Energy Differences and Kinetic Constant Ratios between Termination and Propagation

	ΔE_a[a]		$k_{t,M}/k_p$[b]		k_t^0/k_p[c]	
	vinyl	*trans*-vinylene	GPC	FTIR	GPC	FTIR
Cp	98	76	1.3×10^{-4}	1.9×10^{-4}	0	0
Cp*	41	54	9.0×10^{-4}	4.5×10^{-4}	5.0×10^{-5}	1.3×10^{-5}

[a] $\Delta E_a = E_a^{term} - E_a^{prop}$, in kJ/mol. [b] Dimensionless. [c] Dimension mol/L.

Based on the variation of M_n with monomer pressure, it is not possible to distinguish between the various termination mechanisms that contribute to the monomer independent rate k_t^0. In particular, with L = Cp*, both β-H transfer to Zr and chain transfer to Al may occur. The absence of an increased absorption in the FTIR spectrum at frequencies corresponding to the additional methyl group created in the latter process indicates that β-H transfer to Zr is more important than chain transfer to Al. However, this conclusion is uncertain since analysis of the methyl vibrations is difficult due to overlapping bands. An indication that chain transfer to Al does occur with L = Cp* is provided by the large difference in M_n values determined by FTIR and GPC. With the former method, an estimate of M_n is based on the assumption of one double bond per polymer chain. If termination results in saturated chains, as in chain transfer to Al, M_n as determined by FTIR will be too large since the number of polymer chains is actually larger than the number of double bonds. Chain transfer to aluminum has been observed by others during polymerization with $Cp^*_2ZrCl_2$/MAO.

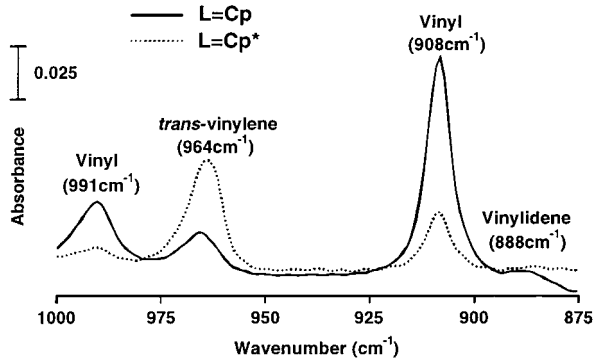

Figure 8. Two representative FTIR spectra of the polyethene obtained by L_2ZrCl_2/MAO (L = Cp, Cp*) catalysis in toluene at $T = 80$ °C and $P_{Ethene} = 1.0$ bar. The spectra show the out-of-plane vibrations of the H-atoms in the unsaturated groups.

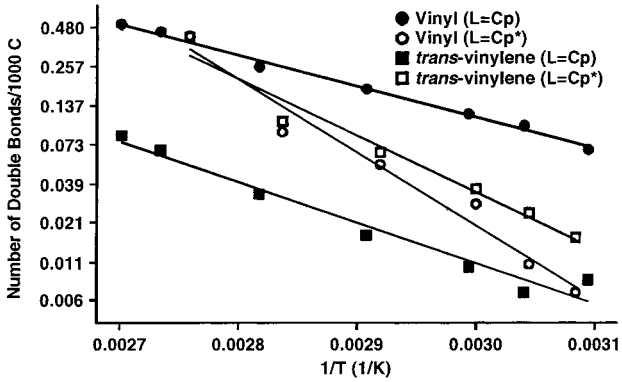

Figure 9. Arrhenius plots of vinyl and *trans*-vinylene unsaturations found in polyethene by FTIR spectroscopy. The polymer was synthesized by L_2ZrCl_2/MAO (L = Cp, Cp*) catalysis in toluene and $P_{Ethene} = 1.0$ bar.

With propene as the monomer, chain transfer to Al was significant only at low temperatures. At $T = 50$ °C, only 1% of the terminations occurred by chain transfer to Al.[22] When 1,5-hexadiene was polymerized at room temperature, chain transfer to Al occurred 4 times as often as β-H elimination.[23]

FTIR of the polymer, e.g., as shown in Figure 8, reveals vinyl and *trans*-vinylene as the two unsaturations found in the polymer. This was also found for L = Cp[19] and heterogeneous $Cp^*_2ZrCl_2$/MAO/SiO_2.[47] Results from the FTIR analysis are listed in Tables 1 and 2, and graphical presentations are given in Figures 9−11. From Figure 8, it is clearly seen that the distribution of unsaturated end groups in the polymers is different depending on the choice of catalyst. This implies that the termination has occurred by different mechanisms, or at least to different extents.

The distribution between the two observable unsaturations is shifted as a function of both pressure and temperature, as shown in Figures 9−11. Assume the number of vinyl or *trans*-vinylene unsaturations per 1000 C atoms to be proportional to the ratio between the kinetic expressions for propagation and termination reactions that result in either of the two unsaturations. Then, it is possible to estimate differences in activation energy between propagation and termination from the Arrhenius plots in Figure 9. Estimates based on our data are given in Table 3.

Figure 10 shows that when the monomer pressure is lowered, the relative vinyl content decreases for both catalysts. The relative vinyl content is the amount of vinyl per 1000 C atoms divided by the total number of

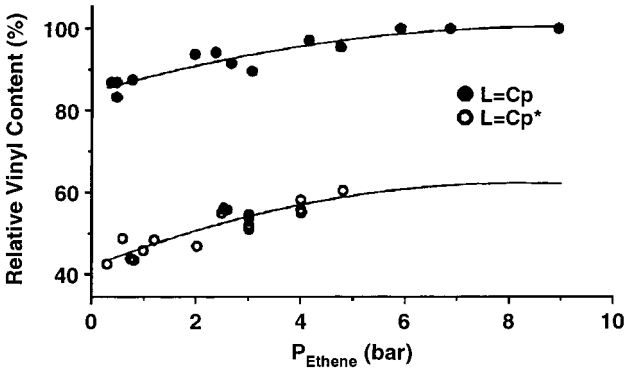

Figure 10. Relative vinyl content in polyethene as a function of monomer pressure. The polymer was synthesized by L_2ZrCl_2/MAO (L = Cp, Cp*) catalysis in toluene and $T = 80$ °C (L = Cp*) and $T = 50$ °C (L = Cp) and analyzed by FTIR. Data for L = Cp from ref 19.

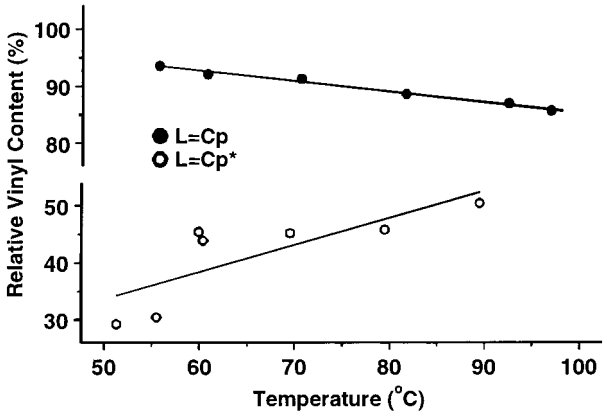

Figure 11. Relative vinyl content in polyethene as a function of reactor temperature. The polymer was synthesized by L_2ZrCl_2/MAO (L = Cp, Cp*) catalysis in toluene and $P_{Ethene} = 1.0$ bar and analyzed by FTIR.

unsaturations per 1000 C atoms. It should be pointed out that L = Cp and L = Cp* were run at $T = 50$ °C and $T = 80$ °C, respectively, but this cannot explain the difference in offset value. This is proven by Figure 11 where we show that a change in polymerization temperature has only a slight effect on the relative vinyl content, and not nearly enough to explain the difference shown in Figure 10. In order to result in a *trans*-vinylene unsaturation after termination, the complex cannot be in the same conformation as when termination yields vinyl unsaturations. On the basis of earlier work on propene polymerization,[26,27] we propose an isomerization to occur according to Scheme 7 followed by termination.[19] We explain the observed pressure dependence by an increase in isomerization as the monomer pressure is lowered. Similar explanations have been used for isomerization during propene polymerization.[26,27,30,31]

Our data indicate that chain isomerization will be followed by termination rather than propagation. Monomer insertion after isomerization would result in single-methyl branches along the polymer backbone, but the FTIR analysis did not show any absorbance at $\nu = 1150$ cm^{-1}. Thus, we conclude that insertion is unlikely after isomerization.

As the temperature is raised from 50 to 97 °C, a small change in the relative vinyl content is observed, as shown in Figure 11. With L = Cp, there is a decrease in the relative vinyl content, and this may be explained by an increasing degree of isomerization prior to ter-

mination as the temperature is raised. With L = Cp*, the vinyl content increases; i.e., there is less isomerization prior to termination as the temperature is raised. Both of these features are in qualitative agreement with the DFT results presented in the next section. For L = Cp, the calculated barrier against isomerization is about 10 kJ/mol higher than against termination by β-H transfer to a monomer and 70 kJ/mol lower than the barrier against termination by β-H transfer to the metal. Thus, an increase in temperature increases the number of isomerizations at the expense of termination by β-H transfer to a monomer. With L = Cp*, the barrier against isomerization is approximately 10 kJ/mol lower than the barriers against termination by β-H transfer to a monomer or to Zr. Hence, an increase in temperature results in an increase in the number of terminations that occur prior to isomerization.

From Table 2, it is seen that the number average molecular weight M_n, as determined by FTIR, is higher with L = Cp* than with L = Cp at $T \leq 80$ °C and opposite at $T = 90$ °C. This should be compared with the results of Kaminsky *et al.*,[34] who obtained a higher viscosity average molecular weight with L = Cp* than with L = Cp at $T = 70$ °C, and those of Ewen,[35] who reported a higher value of the weight average molecular weight M_w with L = Cp than with L = Cp* at $T = 80$ °C. Our results, given in Table 2 and Figure 9, show that the molecular weight of the polyethene is more temperature sensitive with L = Cp* than with L = Cp.

We also performed two experiments with short polymerization times (3 and 6 min), and there was no difference in molecular weight, as determined by FTIR, nor in the distribution of unsaturations between the short-time runs and the runs over 1 h. Thus, the possibility of different termination reactions at different times during polymerization seems unlikely.

From Table 1, it is seen that the M_w/M_n values with L = Cp* deviate considerably from the expected value of 2. This is similar to what has been reported by others.[34,35,47] Kaminsky *et al.*[34] found $6 \leq M_w/M_n \leq 15$ when they used L = Cp* to polymerize ethene at $T = 70$ °C, which is comparable with our values $3.2 \leq M_w/M_n \leq 10$. The polymer obtained with L = Cp has $M_w/M_n = 2.26 \pm 0.08$[19] (see Figure 7B), which is very close to the theoretical value of 2 for single-site catalysis.

5. Results from Quantum Chemical Modeling

We assume that the effect of MAO on the zirconocene dichlorides is to activate the catalyst; i.e., one chloride is substituted with a methyl group and the other is removed, leaving a zirconocene-methyl cation as the starting point for reactions with ethene.[48,49] Any further influence of the MAO is not taken into account, and the catalyst is modeled as a gas-phase molecule. The shielding effect of the aromatic ligands may justify this simplification. Furthermore, the exact structure of MAO in this system is not known, and inclusion of large MAO oligomeric entities would have forced us to use less accurate calculations.[50] The influence of the toluene solvent molecules is in general also neglected (but see section 5.1 below).

We have modeled chain propagation, termination, and isomerization. For each reaction pathway, we present the energy as a function of a chosen reaction coordinate and make direct comparison between the systems with L = Cp and L = Cp*. Molecular structures are shown for important stationary points along some of the linear-transit curves. Additional molecular structures with corresponding energy and structural parameters are available in the Supporting Information (refered to as figures and tables labeled with "S"). A summary of DFT activation energies is included in Table 5.

5.1. Chain Propagation. Starting with $Cp_2ZrCH_3^+$, we have modeled insertion of the first three monomers. In the linear-transit calculations, we have used the C2−C3 distance as the reaction coordinate, i.e., the new bond formed between the monomer and the alkyl chain during the insertion step. Apart from the first insertion, which is a somewhat special case, these reactions represent subsequent insertions to γ-agostic conformations and are well described by Scheme 1. The reaction profiles are shown in Figure 12A, and geometries in stationary points for the first insertion are given in Figure 12C. Related energy and structure parameters can be found in Table 1S.

The calculated reaction energies E_R are similar for the three insertions. The larger value of E_R for the first and second insertion can be explained by differences in agostic bonds in reactants and products. For the first insertion, there is no agostic interaction in the reactant whereas the product is stabilized by an agostic bond between Zr and H_γ. In the second insertion, the agostic bond to the hydrogen on a primary γ-carbon in the reactant is weaker than the bond to the hydrogen on a secondary γ-carbon in the product. This difference in agostic bond strength may be explained in terms of a larger donation of negative charge from the terminal ethyl in $\gamma\text{-}Cp_2ZrC_5H_{11}^+$, than from the terminal hydrogen in $\gamma\text{-}Cp_2ZrC_3H_7^+$. In the third insertion, the reactant and product both have an agostic bond to a hydrogen on a secondary γ-carbon. As a result, the reaction energy is smaller for the third than for the first and the second insertion.

For the reaction profiles, there are remarkable differences. In the first insertion, the ethene complexation is much stronger than in subsequent insertions. We ascribe this difference to the lack of stabilizing agostic interactions in the methyl cation $Cp_2ZrCH_3^+$. In this cation, zirconium has an essentially vacant coordination site that is readily occupied by a monomer. Actually, the methyl cation is structurally very little changed during the formation of the π-complex **12**−**1**, with, e.g., no α-agostic interaction. In contrast, the α-agostic π-complexes of the second and third insertion bear little resemblance of the corresponding γ-agostic reactants. In this case, ethene complexation requires that the agostic bond in the reactant is broken. This results in a lower complexation energy and, for the third insertion, even a small barrier against monomer complexation. All three insertion reactions pass through a four-center α-agostic transition state. For the first insertion, the structural differences between the π-complex **12**−**1** and the transition state **12**−**2** are much larger than for subsequent insertions. As a consequence, the insertion barrier is substantially higher for the first insertion.

The typical insertion is believed to be well represented by the reaction $\gamma\text{-}Cp_2ZrC_5H_{11}^+ + C_2H_4 \rightarrow \gamma\text{-}Cp_2ZrC_7H_{15}^+$. It is characterized by a mainly flat potential energy surface before reaching a shallow energy minimum due to the ethene complex, followed by insertion with an energy barrier of about 10 kJ/mol. The first insertion is different from subsequent ones, with an

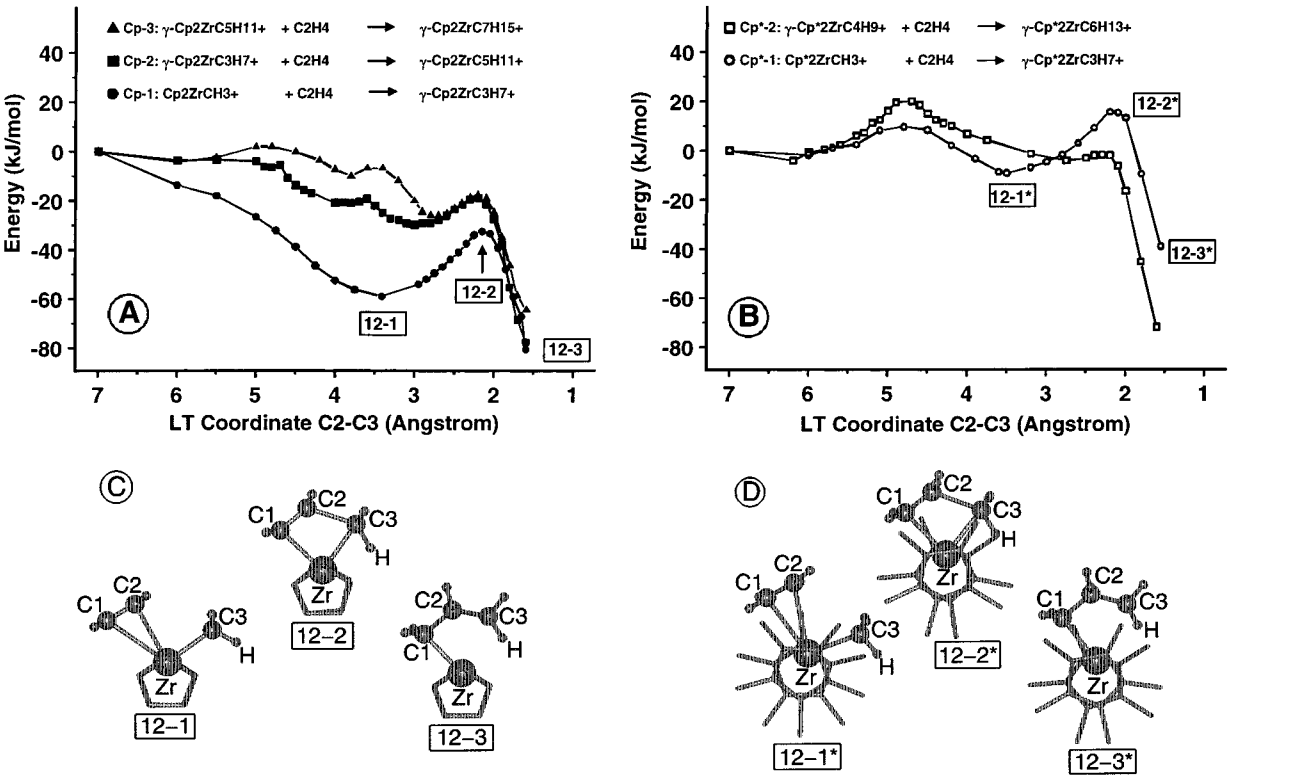

Figure 12. First insertion and subsequent insertions to γ-agostic structures according to Scheme 1: (A) reaction profiles for first three insertions with L = Cp; (B) reaction profiles for first and typical insertion with L = Cp*; (C) geometry of π-complex, transition state, and γ-agostic product for first insertion with L = Cp; (D) same as (C) with L = Cp*.

energy barrier of 26 kJ/mol. This has motivated the inclusion of the initiation reaction in the kinetic model discussed earlier (Scheme 8, eq 1).

Figure 12B shows the reaction profiles for two insertion reactions with L = Cp*, one corresponding to the first insertion with a methyl starting group, and the other representing the typical insertion reaction with a butyl starting group. Stationary point geometries for the first insertion are given in Figure 12D, and related energy and structure parameters can be found in Table 1S.

Surprising at first, the reaction energy E_R of the first insertion is much smaller than for subsequent insertions with L = Cp*, and only half the value calculated with L = Cp. This difference may be explained in terms of steric repulsion: The L−Zr−L angle is 3−4° larger in the $L_2ZrCH_3^+$ cations than in all the γ-agostic products. The presence of an alkyl chain longer than methyl results in a smaller L−Zr−L angle and, consequently, a closer approach of the two ligands at the narrow side. With bulky methyl substituents on the Cp* ligands, the resulting energy cost is much higher than with small hydrogens on the Cp ligands. The smallest H−H distances are also indicative of steric repulsion in the γ-agostic products with L = Cp*. Therefore, compared with the γ-agostic propyl cation, the methyl cation is relatively more stable with L = Cp* than with L = Cp, and this explains the calculated difference in E_R between the two catalysts for the first insertion. These considerations do not apply to the second reaction since reactant and product then have essentially the same γ-agostic configuration. Hence, the calculated reaction energy is similar for insertion into γ-Cp*$_2$ZrC$_4$H$_9^+$ and γ-Cp$_2$ZrC$_5$H$_{11}^+$, −72 and −64 kJ/mol, respectively. These numbers compare favorably with the experimental value of −82 kJ/mol, where the latter is based on the difference in bond dissociation energy of the single and double carbon−carbon bond.[51]

For both reaction profiles in Figure 12B, there is an energy barrier against complexation of the monomer. In the first insertion, this barrier is ascribed to steric repulsion between the approaching monomer and the nearest methyl groups on the Cp* ligands. For insertion to the γ-agostic butyl cation, we ascribe the early barrier both to steric repulsion and to breaking the agostic bond in the reactant. As found for L = Cp, the π-complex **12−1*** of the first insertion is structurally far more different from the transition state **12−2*** than is the case for subsequent insertions. Hence, the second barrier is again considerably higher for the first insertion. For insertion to γ-Cp*$_2$ZrC$_4$H$_9^+$, the second barrier is only 2 kJ/mol, and the rate-determining step is the ethene complexation, with a barrier of about 24 kJ/mol.

A γ-agostic structure may undergo a rotation of the alkyl chain and reach a more stable β-agostic conformation (Scheme 2). In Figure 13, we present the results of linear-transit calculations along a reaction path where the dihedral angle Zr−C$_\alpha$−C$_\beta$−C$_\gamma$ is used as the LT coordinate. Molecular structures **13−1** and **13−1*** can be found in Figure 1S and correspond to the transition states for the rotation with L = Cp and L = Cp*, respectively.[52,53] In Table 2S, related energies and structure parameters are included. The agostic interaction between Zr and H$_\beta$ in the β-agostic conformation is stronger than the one between Zr and H$_\gamma$ in the γ-agostic conformation. This is reflected in a shorter Zr−H$_\beta$ and a longer C$_\beta$−H$_\beta$ distance. Contrary to what one might expect, the energy barrier for the $\gamma \rightarrow \beta$ rotation is not much higher with L = Cp* than with L = Cp, 15 vs 11 kJ/mol. The rotation reaction is only slightly hindered by the bulky methyl groups on the Cp* ligands. This is illustrated by the relatively small

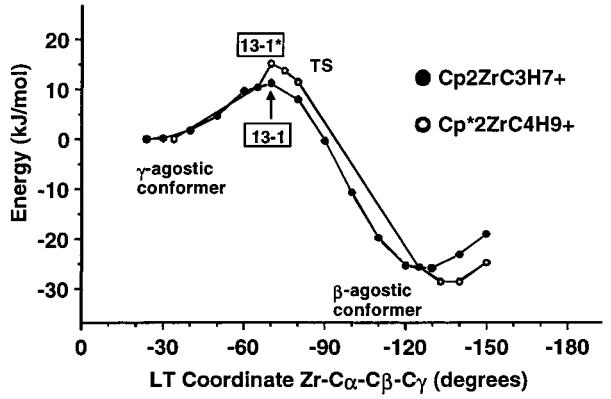

Figure 13. Reaction profiles for the rotation between γ- and β-agostic conformations of $Cp_2ZrC_3H_7^+$ and $Cp^*_2\ ZrC_4H_9^+$ according to Scheme 2.

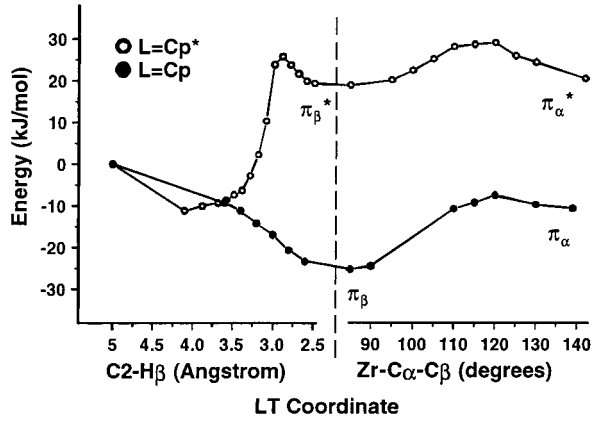

Figure 14. Frontside insertion to β-agostic structures $Cp_2ZrC_3H_7^+$ and $Cp^*_2ZrC_4H_9^+$ according to Scheme 3. Reaction profiles for the formation of a β-agostic π-complex (left half) and reorientation to an α-agostic π-complex (right half).

changes in the opening angle L−Zr−L and the shortest H−H distances during the rotation reaction. The steric repulsion, already present in the γ-agostic minimum of $Cp^*_2ZrC_4H_9^+$, is only negligibly stronger in the transition state **13−1*** . Since the energy barrier is low in both cases, a large number of active sites is expected to be in their β-agostic ground state, especially if the monomer pressure is low.

As pointed out by Lohrenz *et al.*[9], a β-agostic structure may serve as the starting point for a number of reactions. We have investigated frontside and backside monomer insertion, as illustrated in Schemes 3 and 4, both with L = Cp and L = Cp*. In Figures 14 and 15, the linear-transit energy profiles are shown for reaction paths corresponding to frontside and backside approaches, respectively, starting from the β-agostic conformations of $Cp_2ZrC_3H_7^+$ and $Cp^*_2ZrC_4H_9^+$.[53] In Table 3S, corresponding energy and structure parameters can be found.

Frontside insertion is modeled in two steps. Complexation of ethene is modeled with the C2−H_β distance as the LT coordinate, whereas the rotation from β-agostic to α-agostic π-complex is modeled with the Zr−C_α−C_β angle as the LT coordinate.[54] With L = Cp, formation of the β-agostic π-complex (π_β in Figure 14) proceeds without hindrance. For the $\pi_\beta \rightarrow \pi_\alpha$ rotation, there is an energy barrier of 18 kJ/mol. This is the dominating barrier, since insertion from the α-agostic π-complex was already found to take place with a barrier of less than 10 kJ/mol (Figure 12A). With L = Cp*, a dominating energy barrier of 37 kJ/mol is found for the complexation of ethene (π^*_β in Figure 14). Again, one observes the effect of steric repulsion when the monomer passes the bulky methyl groups of the Cp* ligands. Rotation from π^*_β to π^*_α has a low barrier of only 10 kJ/mol, and the final insertion barrier was found to be negligible (2 kJ/mol).

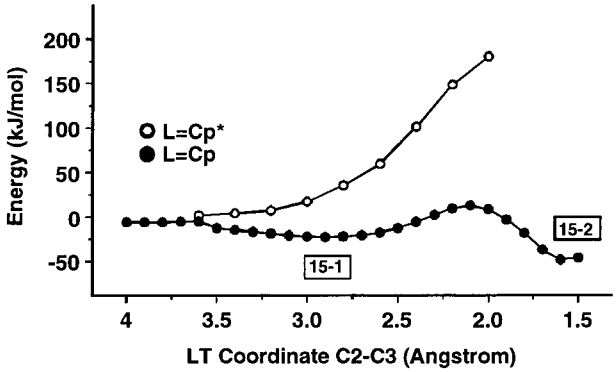

Figure 15. Reaction profiles for the backside insertion to β-agostic structures $Cp_2ZrC_3H_7^+$ and $Cp^*_2ZrC_4H_9^+$ according to Scheme 4.

Backside insertion is modeled with the C2−C3 distance as the LT coordinate. With L = Cp, complexation of the monomer (**15−1**) is unhindered, and monomer insertion and formation of a δ-agostic product (**15−2**) proceeds with an activation energy of 36 kJ/mol. Molecular structures can be found in Figure 2S. With L = Cp*, the energy increases steadily along the linear-transit path, and a stable π-complex could not be found. The insertion barrier appears to be very high, at least 180 kJ/mol. The methyl groups of the Cp* ligands effectively block the entrance and prevent monomer insertion.

In an attempt to account for the large propagation activation energy observed for L = Cp, we have tried to assess a possible influence of the solvent on chain propagation. Specifically, we have optimized the geometries of a toluene molecule coordinated to β-agostic $L_2ZrC_3H_7^+$. With L = Cp, a π-complex is formed where one of the C−C bonds of the aromatic 6-ring is coordinated to Zr with Zr−C distances below 3 Å. The binding energy of about −15 kJ/mol is only 10 kJ/mol smaller and the Zr-olefin distance is only about 20 pm longer than for π-complexation of ethene. With L = Cp*, a weakly bound adduct is formed, with Zr−C distances around 5 Å. As expected, the methyl substituents of the Cp* ligands prevent strong coordination of the solvent. These results indicate that reactions with ethene may be more influenced by the solvent with L = Cp than with L = Cp* and may, at least partly, account for the large experimental activation energy observed for chain propagation with the Cp-based catalyst.

In summary, propagation of the polyethene chain may start from both β- and γ-agostic conformations. For the two catalysts $L_2Zr\text{-alkyl}^+$ with L = Cp and L = Cp*, we note the following similarities and discrepancies concerning insertion into γ-agostic structures:

- The overall reaction energies are similar, as expected. (For infinitely long chains, they must necessarily be identical.)
- In both cases, there is an energy minimum corresponding to the complexation of ethene, and energy barriers before and after the complexation.

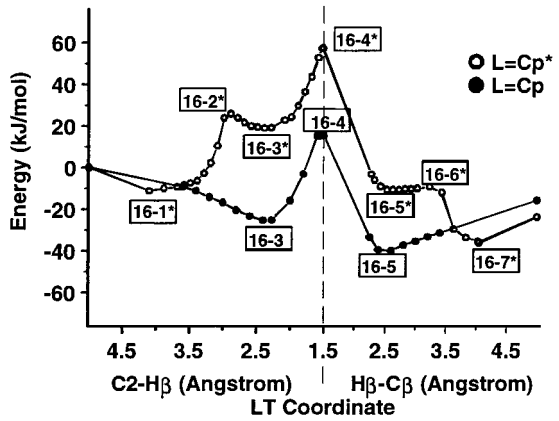

Figure 16. Reaction profiles for termination via transfer of a β-hydrogen to a coordinated monomer from $Cp_2ZrC_3H_7^+$ and $Cp^*_2ZrC_4H_9^+$ according to Scheme 5.

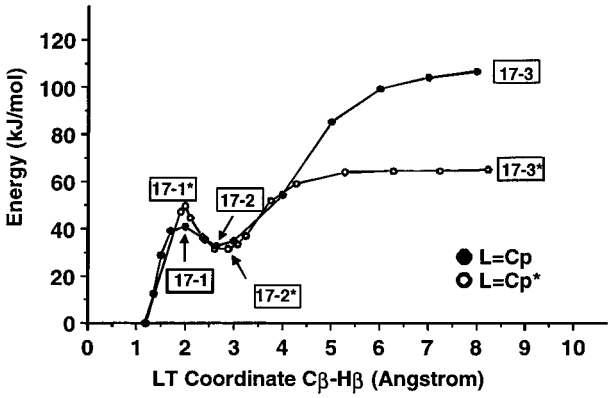

Figure 17. Reaction profiles for termination via transfer of a β-hydrogen to zirconium in $Cp_2ZrC_3H_7^+$ and $Cp^*_2ZrC_4H_9^+$ according to Scheme 6.

•With L = Cp, both barriers are small, only 6−8 kJ/mol.

•With L = Cp*, the complexation barrier of about 24 kJ/mol is dominating, whereas the second barrier is negligible, only about 2 kJ/mol.

We note further

•Reorientation of the alkyl chain from a γ- to a β-agostic conformation has a low energy barrier of 10−15 kJ/mol for both catalysts and is surprisingly little hindered by the bulky Cp* ligands. The β-agostic structures are stabilized relative to the γ-agostic ones by 26−28 kJ/mol.

•Frontside insertion to β-agostic conformations is possible for both catalysts studied. With L = Cp, the highest barrier (18 kJ/mol) is found for the rearrangement from a β-agostic to an α-agostic π-complex. With L = Cp*, complexation of ethene is the rate-determining step with a barrier of 37 kJ/mol.

•Backside insertion to a β-agostic conformation is very unlikely for L = Cp*. For L = Cp, the insertion barrier of 36 kJ/mol is higher than for frontside insertion.[55]

•The β-agostic ground state is a rather stable structure, in particular with L = Cp*. It is a "latent site", prone to a number of competing reactions, including propagation, $\beta \rightarrow \gamma$ rotation, isomerization, and termination.

•Coordination of a solvent molecule is found to be stronger with L = Cp than with L = Cp* and is therefore expected to have a larger influence on the polymerization rate in the former case.

5.2. Chain Termination. It is natural to consider termination mechanisms that originate from a β-agostic structure, since this is the ground state in these systems.[56] We have modeled two mechanisms that involve transfer of a β-hydrogen:

•transfer of H_β to a coordinated monomer (Scheme 5)

•transfer of H_β to the metal (Scheme 6)

Reaction profiles for these processes are shown in Figures 16 and 17, respectively, with selected geometries included in Figures 3S and 4S. Energies of stationary points along the linear-transit curves can be found in Table 4S.

Transfer of H_β to a coordinated monomer involves the same monomer complexation as modeled in Figure 14, i.e., with no energy barrier for L = Cp and a steric barrier of 37 kJ/mol for L = Cp*. From the β-agostic π-complexes **16**−**3** and **16**−**3***, the reactions proceed with transfer of the hydrogen through transition states **16**−**4** and **16**−**4*** . This part of the reaction is very similar for the two catalysts, with energy barriers of about 40 kJ/mol. When the hydrogen has been transferred to the monomer, another π-complex (**16**−**5**, for L = Cp) is reached where the terminated chain is coordinated to a β-agostic ethyl cation. With L = Cp, removal of the coordinated chain (here: propene) is endothermic by 23 kJ/mol, and the total reaction energy is −16 kJ/mol. With L = Cp*, removal of the coordinated chain (here: 1-butene) follows a similar pattern as the initial monomer approach; i.e., a global energy minimum **(16**−**7*)** is reached when the terminated chain is well outside the methyl groups of the Cp* ligands. The total reaction energy in this case is −24 kJ/mol. On the basis of the reaction profiles in Figure 16, we find that the total energy barrier for β-H transfer to a coordinated monomer is 41 kJ/mol with L = Cp and 68 kJ/mol with L = Cp*.

Transfer of H_β to zirconium has been modeled by others[13,16] and found to be rather strongly endothermic. Our results agree with this, and we find that the β-agostic $Cp_2ZrC_3H_7^+$ is 113 kJ/mol more stable than the products Cp_2ZrH^+ and propene. With L = Cp*, the situation is different, since β-$Cp^*_2ZrC_4H_9^+$ is only 64 kJ/mol more stable than $Cp^*_2ZrH^+$ and 1-butene. In Figure 17, results of the LT calculations are shown for this reaction. Notice that there is a local minimum on the energy curve where the olefin-like chain is coordinated to the zirconocene hydride (**17**−**2** and **17**−**2***). This minimum is reached after passing through transition states **17**−**1** and **17**−**1*** with activation energies of 42 and 50 kJ/mol with L = Cp and L = Cp*, respectively. Compared with separate products, the complexes **17**−**2** and **17**−**2*** have binding energies −79 kJ/mol with L = Cp and only −21 kJ/mol with L = Cp*. This result agrees with what we found above, that coordination of an olefin to a Cp*-based catalyst is in general less favorable than with a Cp-based structure.

Note that β-hydride elimination is calculated to be more unfavorable when starting with an ethyl chain. The reaction energies are 126, 113, and 115 kJ/mol with L = Cp when starting with an ethyl, propyl, and butyl chain, respectively. For L = Cp*, the corresponding numbers are 88, 65, and 64 kJ/mol. The origin of the difference between ethyl and the longer chains is simply the difference in reaction enthalpy during saturation of an olefinic double bond, which is −137 kJ/mol for ethene and about −125 kJ/mol for propene and longer α-olefins.[57] Due to more steric repulsion in the reactant than in the products, β-hydride elimination becomes less endothermic with L = Cp* than with L = Cp. It appears

that a propyl chain is necessary, and also sufficient, to model the typical β-hydride elimination.

One could imagine a combined mechanism where chain termination takes place via first partial transfer of H_β to the metal and subsequently to an incoming monomer while the terminated chain is still coordinated to the catalyst. We have attempted to model such a mechanism, starting from the local minimum **17**−**2** and introducing an additional ethene molecule. This leads to immediate reinsertion of the coordinated chain, i.e., with the π -complex **16**−**3** as the resulting geometry, and not **16**−**5** as anticipated. Therefore, we consider such a combined termination mechanism as unlikely.

Let us summarize what we have found for the termination reactions based on β-H transfer:

•The catalyst with L = Cp has energy barriers of 41 kJ/mol for transfer of H_β to a coordinated monomer and 115 kJ/mol for transfer of H_β to zirconium. We expect the former mechanism to be most important for this catalyst.

•The catalyst with L = Cp* has energy barriers of 68 kJ/mol for transfer of H_β to a coordinated monomer and 64 kJ/mol for transfer of H_β to zirconium. We expect both mechanisms to be about equally important for this catalyst.

5.3. Chain Isomerization and Polymer Unsaturations. Isomerization. The isomerization reaction has been modeled according to Scheme 7 for the two catalysts. Starting from β-agostic structures, the isomerization is completed in three steps: (1) partial transfer of the β-hydrogen to zirconium, (2) a relative rotation of the hydride and the coordinated olefin, and (3) reinsertion of the olefin into the Zr−H bond.

In Figure 18A, reaction profiles are shown for the complete isomerization path. Minimum-energy structures are included in Figure 18B, and in Table 4 we have collected important energies and structure parameters.

The main impression from Figure 18A is that the isomerization reaction is energetically very similar for the two catalysts. The rate-determining step is clearly the initial transfer of the β-hydrogen to the metal, with energy barriers of 42 and 50 kJ/mol with L = Cp and L = Cp*, respectively. The relative hydride-olefin rotation is almost free in both cases (ΔE = 10 and 13 kJ/mol for L = Cp and L = Cp*, respectively), and reinsertion of the olefin also proceeds with a low energy barrier of about 6 and 13 kJ/mol for L = Cp and L = Cp*, respectively.

This is another example of a reaction that involves a rotation where the steric influence of the Cp* ligands is surprisingly low. The relative hydride-olefin rotation requires a substantial increase in the Zr−C1−C2 angle, in particular with L = Cp* (Table 4). However, since the olefin is rather weakly bonded in the complexes **18**−**2** and **18**−**2***, the potential-energy surface is almost flat along the rotation reaction.

With L = Cp, the direct product **18**−**6** of the linear−transit calculation has two β-agostic bonds, between Zr and H2 on the primary β-carbon (C1) and between Zr and H3 on the secondary β-carbon (C3). As expected, the latter bond is the stronger, with a shorter Zr−H and a longer C−H distance, as seen from Table 4. With L = Cp*, the direct product **18**−**6*** has only one β-agostic bond to H2 on the primary β-carbon (C1). The two isomers are only slightly less stable than the initial structures, 15 and 10 kJ/mol for L = Cp and L = Cp*, respectively.

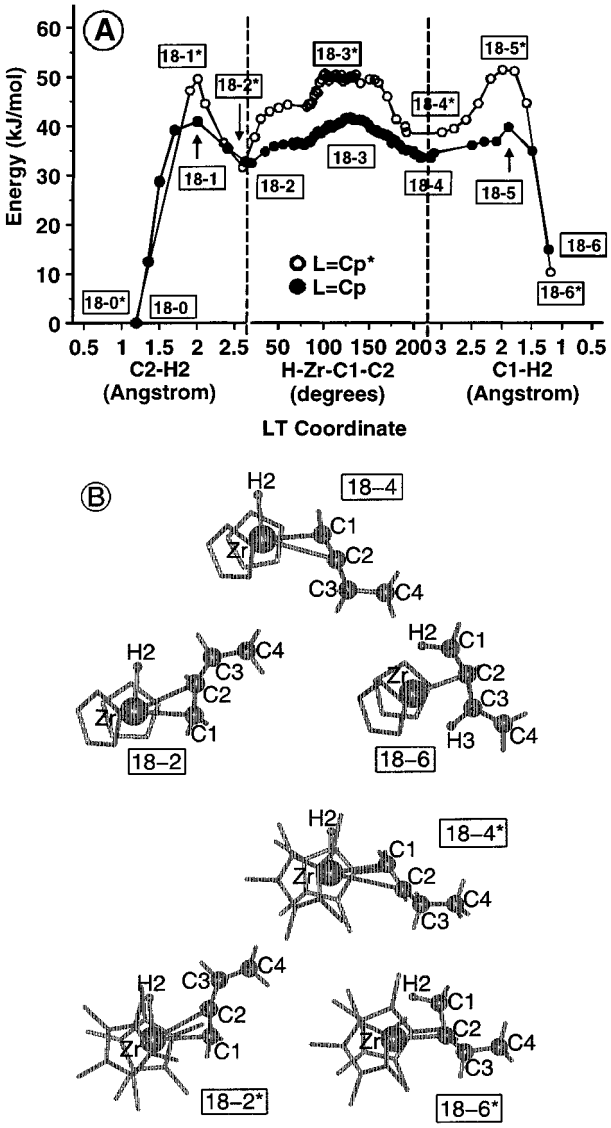

Figure 18. Isomerization of $Cp_2ZrC_4H_9^+$ and $Cp^*_2ZrC_4H_9^+$ according to Scheme 7: (A) reaction profiles for partial transfer of H_β to Zr (left part), relative rotation of hydride and olefin (middle part), and reinsertion of the olefin into the Zr−H bond (right part); (B) geometry of initial hydride−olefin complexes (**18**−**2** and **18**−**2***), rotated hydride−olefin complexes (**18**−**4** and **18**−**4***), and isomer products (**18**−**6** and **18**−**6***).

Rotation between β-Agostic Conformations. After isomerization, different β-agostic conformations are possible. We have modeled rotation reactions between structures with agostic hydrogens on either or both β-carbons. The reaction profiles are presented in Figure 19, and minimum-energy structures can be found in Figure 5S. As the linear-transit coordinate, we have used the dihedral angle θ_1 = Zr−$C_{\beta1}$−C_α−$C_{\beta2}$ or θ_2 = Zr−$C_{\beta2}$−C_α−$C_{\beta1}$. In the conformation 2β with two agostic interactions, θ_1 and θ_2 are both close to 80°. By increasing θ_1, the agostic bond to $H_{\beta2}$ is broken, and the conformation β1 with an agostic hydrogen on the primary β-carbon is reached at $\theta_1 \simeq 120-130°$. Analogously, if θ_2 is increased, the conformation β2 with an agostic hydrogen on the secondary β-carbon is reached at $\theta_2 \simeq 120-130°$.

In Table 5S, we have collected the energies of the different conformers and approximate transition states between them. All the rotational barriers are low, in the range 9−23 kJ/mol. Furthermore, the various

Table 4. DFT Results for the Isomerization Reaction with L = Cp and L = Cp*

	L = Cp[a]							L = Cp*						
	0	1[b]	2	3	4	5	6	0*	1*	2*	3*	4*	5*	6*
energy[c]	0	42	32	42	34	40	15	0	50	43	56	39	51	9
structure[d]														
Zr−C1	2.31	2.51	2.60	2.63	2.58	2.67	2.63	2.32	2.50	2.64	2.67	2.70	2.79	2.64
Zr−C2	2.67	2.82	3.01	3.33	3.19	2.55	2.39	2.68	2.80	3.05	3.51	3.43	2.73	2.36
Zr−C3	3.92	3.84	3.97	4.22	4.20	2.75	2.64	3.99	3.92	4.03	4.54	4.67	3.68	3.51
Zr−H2	2.17	1.91	1.89	1.88	1.88	1.90	2.15	2.18	1.92	1.89	1.88	1.88	1.88	2.14
Zr−H3				4.47	4.32	2.22	2.10				4.52	4.87	3.74	3.67
C2−H2	1.20	2.00	2.64	4.26	4.24	2.72		1.20	2.00	2.88	4.07	4.18	2.89	
C1−H2				3.28	3.18	1.90	1.22				3.24	2.96	2.00	1.19
C3−H3	1.12	1.11	1.12	1.12	1.12	1.18	1.24	1.12	1.11	1.11	1.12	1.12	1.12	1.12
Zr−C1−C2	86	88	93	109	103	70	64	86	87	94	117	111	73	63
L−Zr−L	138	136	135	133	134	132	131	141	140	139	138	140	138	139
H−Zr−C1−C2	5	2	9	129	207	209	205	8	13	24	101	191	178	176

[a] Numbers 0−6 and 0*−6* refer to stationary points along the isomerization path in Figure 18A for L = Cp and L = Cp*, respectively. [b] Values obtained with propyl chain. [c] Relative to the initial β-agostic structures 0 and 0*, in kJ/mol. [d] Bond lengths in Angstrom, angles in degrees. See Figure 18B. L: center of C_5 ring.

Table 5. Summary of Activation Energies (in kJ/mol) Derived from DFT Calculations

type of reaction	figure with LT curves	activation energies	
		L = Cp	L = Cp*
insertion to γ-agostic structure	12A−B	8	24
rotation from γ- to β-agostic structure	13	11	15
insertion to β-agostic structure (frontside approach)	14	18	37
insertion to β-agostic structure (backside approach)	15	36	>180
termination by β-H transfer to coordinated monomer	16	41	68
termination by β-H transfer to Zr	17	115	64
alkyl chain isomerization	18A	42	50
rotation between β-agostic conformers	19	≤12	≤23
termination by β-H transfer to coord. monomer after isomerization	20A	40	75
termination by β-H transfer to Zr after isomerization		90−100	∼50

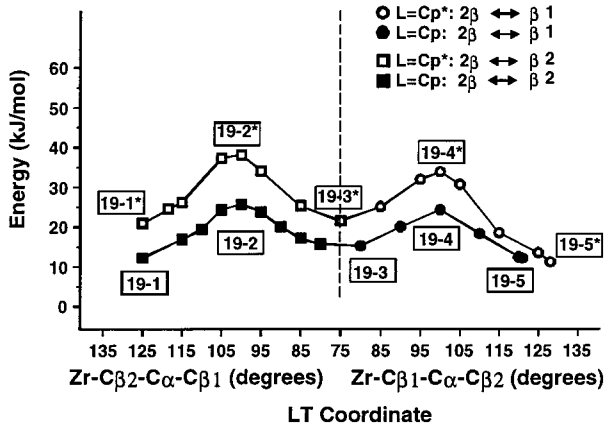

Figure 19. Reaction profiles for rotation between β-agostic conformations of the isomer products in Figure 18B.

conformations have small energy differences, less than 11 kJ/mol.

Consequences for Termination and Polymer Unsaturations. The small energy barriers and energy differences between the β-agostic conformations presented above indicate that they may be in or close to thermodynamic equilibrium after an isomerization reaction. As a consequence, chain termination may occur via transfer of a β-hydrogen from either the primary or the secondary β-carbon. The terminated polymer chain will have different end groups in the two cases: Transfer of $H_{\beta 1}$ from the primary $C_{\beta 1}$ yields a vinyl-terminated chain, whereas transfer of $H_{\beta 2}$ from the secondary $C_{\beta 2}$ results in a chain with a *trans*-vinylene end group.

Chain propagation is assumed to be unlikely after isomerization, since the additional alkyl group on C_α is expected to raise the energy barrier for the π_β to π_α reaction (see section 5.1) and suppress the rate of propagation. This assumption is consistent with the FTIR spectra, which do not reveal single-methyl branches along the polymer backbone.

We have performed linear-transit calculations for termination by transfer of H_β to a coordinated monomer, starting from the $\beta 1$ and $\beta 2$ conformations of $L_2ZrC_4H_9^+$ with L = Cp and L = Cp*. The reaction profiles are shown in Figure 20A, and the four minimum-energy structures obtained after hydrogen transfer to the monomer are presented in Figure 20B. Table 6S contains related energy values. For termination by transfer of H_β to zirconium, we have only calculated the energy differences between the β-agostic reactants and the products, which are the L_2ZrH^+ hydride and C_4H_8 (1-butene or *trans*-2-butene). These results are also included in Table 6S.

The LT curves in Figure 20A for the $H_\beta \rightarrow$ monomer reactions are very similar to the corresponding curves in Figure 16, which represent the analogous termination reactions prior to chain isomerization. The only difference is essentially a global shift upward of the linear-transit curves by 10−20 kJ/mol, reflecting the total reaction energies of the isomerization reactions. Thus, the energy barriers calculated for chain termination, 75−85 kJ/mol with L = Cp* and 35−40 kJ/mol with L = Cp, are not much different from the corresponding values of 68 and 41 kJ/mol found for the analogous termination reactions prior to isomerization. Although we have not performed the linear-transit calculations for removal of the coordinated olefins in the π -complexes of Figure 20B, we have verified that these structures are more stable than the separate products with L = Cp and less stable with L = Cp*, in agreement with the results in Figure 16. As expected, removal of

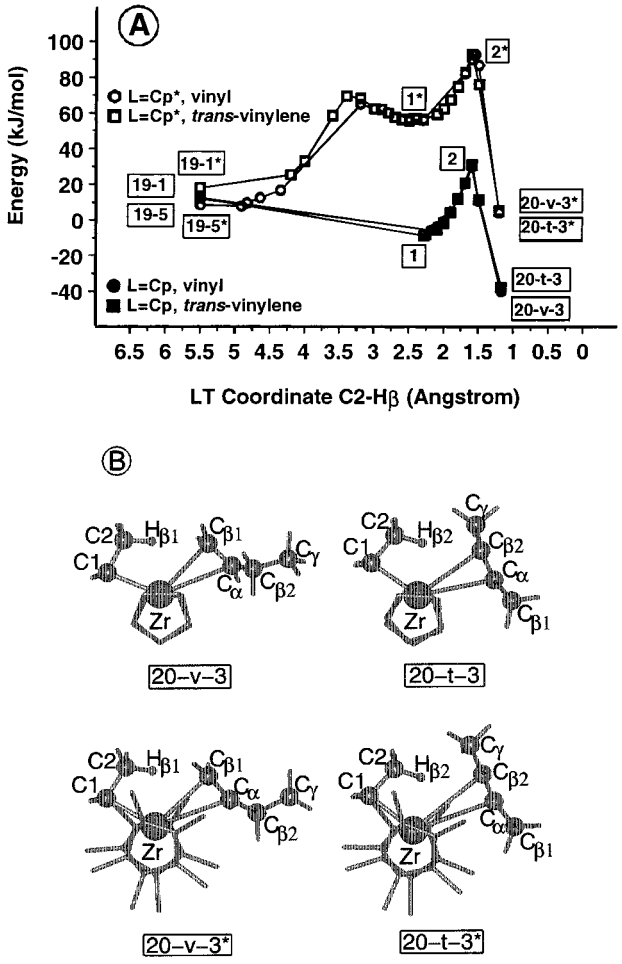

Figure 20. Termination via transfer of β-hydrogen to coordinated monomer from $\beta 1$ and $\beta 2$ conformations of $Cp_2ZrC_4H_9^+$ and $Cp^*_2ZrC_4H_9^+$: (A) reaction profiles; (B) geometry of π-complexes reached after hydrogen transfer, with coordinated 1-butene (**20-v-3** and **20-v-3***) and *trans*-2-butene (**20-t-3** and **20-t-3***).

trans-2-butene is easier than 1-butene, both because *trans*-2-butene is a more stable molecule than 1-butene, and also because coordination of the former implies more steric strain.

The π -complexes in Figure 20B clearly show the different end groups: In **20-v-3** and **20-v-3*** , the terminated chain has a vinyl unsaturation, whereas in **20-t-3** and **20-t-3*** , we obtain a *trans*-vinylene end group.

Due to less stable reactants, the reaction energies for termination via transfer of H_β to the metal are lower now than before isomerization. In particular, the reaction energy for $\beta 2\text{-}Cp^*_2ZrC_4H_9^+ \rightarrow Cp^*_2ZrH^+ +$ *trans*-2-butene is only 31 kJ/mol. In this case, we expect that the activation energy is given by the barrier against transfer of H_β to Zr and formation of the complex with the olefin coordinated to the zirconocene hydride, about 50 kJ/mol. This is lower than the activation energy found for transfer of H_β to a coordinated monomer, so we expect β-hydride elimination to be the most important termination mechanism after isomerization with L = Cp*. With L = Cp, β-hydride elimination still has an activation energy that is significantly higher than for transfer of H_β to a monomer. Therefore, the latter is expected to be the dominating termination mechanism with L = Cp, also after isomerization.

Most important, however, is the demonstration of a viable reaction sequence, which results in *trans*-vinylene unsaturation, namely alkyl chain isomerization followed by termination via transfer of a β-hydrogen from the secondary β-carbon. The mechanism is demonstrated for both catalysts studied, and appears to be at least as relevant for L = Cp* as for L = Cp.

6. Conclusions

Based on our results for ethene polymerization with the two catalyst systems L_2ZrCl_2/MAO with L = Cp and L = Cp*, the following conclusions may be drawn:

1. The experiments have revealed certain striking differences between the two catalyst systems. First, in the average molecular weight, which is found to be independent of monomer pressure up to 9 bar with L = Cp, whereas with L = Cp*, it increases with increasing pressure up to about 2 bar and remains constant thereafter. Second, in the composition of polymer unsaturation, which is strongly dominated by vinyl with L = Cp, whereas with L = Cp*, the amounts of vinyl and *trans*-vinylene are approximately equal. Third, in the average polymerization activity as a function of temperature, which increases monotonically between 10 and 97 °C with L = Cp, whereas with L = Cp*, a maximum value is found at about 45 °C.

2. During our polymerization experiments, the activity is not constant. The time profile may be described by a reaction scheme that involves catalyst activation, chain propagation, and catalyst deactivation. As a result, the temperature dependence of the average catalytic activity depends on the polymerization time. This makes, e.g., a determination of activation energies difficult without kinetic modeling. By fitting the activity time profiles with a simple kinetic model, a rate constant k_2 for propagation has been determined. The corrected activity based on k_2 increases with increasing temperature for both catalysts and results in experimental activation energies of 61 and 17 kJ/mol for chain propagation with L = Cp and L = Cp*, respectively. Taking the various propagation mechanisms into account, the corresponding (electronic) activation energies derived from DFT calculations are 10−20 kJ/mol for L = Cp and 25−35 kJ/mol for L = Cp*. The agreement for Cp* is reasonable, whereas for Cp it is not. One reason for this could be that the Cp experiments are more influenced by the surroundings, i.e., the solvent and MAO, which are not taken into account in the DFT calculations. In fact, solvent effects that mainly will influence polymerization with L = Cp are suggested by preliminary DFT calculations. Limitation by diffusion appears to be unlikely, but cannot be completely ruled out.

3. The pressure dependence observed for the average molecular weight indicates that chain termination occurs by transfer of a β-hydrogen to the zirconium center and to a coordinated monomer for L = Cp*. For L = Cp, termination happens predominantly by β-hydrogen transfer to a coordinated monomer. This interpretation of the experimental data is strongly supported by the DFT calculations. Chain transfer to Al in MAO is an alternative termination mechanism that may account for the big difference in average molecular weight determined by FTIR and GPC analysis of the polymer produced with L = Cp*.

4. Based on the temperature dependence of the molecular weight, it is possible to estimate the difference

ΔE_a between activation energies for termination (or isomerization) and propagation. The experimental ΔE_a values are 40−50 kJ/mol for L = Cp and 75−100 kJ/mol for L = Cp*. Based on DFT calculations, we estimate somewhat smaller ΔE_a values, 20−30 and 30−40 kJ/mol, respectively. The discrepancy between experiment and theory is large for L = Cp*, but in that case the experimental value is also less certain.

5. The distribution of unsaturation in the polymer is very different with L = Cp and L = Cp*. With L = Cp*, we find approximately a 1:1 distribution between *trans*-vinylene and vinyl, whereas with L = Cp, the corresponding distribution is 1:6 or higher. We ascribe this difference to a higher degree of isomerization with L = Cp* than with L = Cp. This interpretation is supported by the DFT calculations by comparing the energy barriers for isomerization and termination. For L = Cp*, the isomerization barrier (50 kJ/mol) is lower than the termination barrier (65 kJ/mol), whereas for L = Cp, the two barriers are almost equal (42 and 41 kJ/mol).

6. Various types of agostic interactions appear to be a crucial ingredient in virtually all reactions that we have studied. The presence of an agostic bond is a natural consequence of the free coordination site at the metal center and its electron-deficient nature. In particular, the ground state of an L_2Zr-alkyl$^+$ cation is always found to be a β-agostic conformation. Varying with the type of ligand L, the β-agostic ground state may have relatively high energy barriers for the various reactions with a monomer. On the basis of this, we suggest that it could represent so-called latent (or dormant) sites in some of these systems.

7. Contrary to our initial expectations, we have found that most reactions that involve a rotation or rearrangement of the alkyl chain close to the metal are *not* hindered by the bulkier Cp* ligands. This has been demonstrated in several calculations, and also experimentally by the large degree of isomerization observed with the Cp* based catalyst.

Acknowledgment. Financial support from the Norwegian Research Council (NFR) under the Polymer Science Program and Borealis is gratefully acknowledged. GPC measurements by H. N. Bryntesen at Borealis, Rønningen, Norway, are acknowledged.

Supporting Information Available: Figures of molecular structures and tables with energies and geometric parameters derived from DFT calculations (5 pages). Ordering and accessing information is given on any current masthead page.

References and Notes

(1) Kaminsky, W. *Catal. Today* **1994**, *20*, 257−271.
(2) Möhring, P. C.; Coville, N. J. *J. Organomet. Chem.* **1994**, *479*, 1−29.
(3) Gupta, V. K.; Satish, S.; Bhardwaj, I. S. *J. Macromol. Sci., Rev. Macromol. Chem. Phys.* **1994**, *C34* (3), 439−514.
(4) Brintzinger, H. H.; Fischer, D.; Mülhaupt, R.; Rieger, B.; Waymouth, R. M. *Angew. Chem., Int. Ed. Engl.* **1995**, *34*, 1143−1170.
(5) Bochmann, M. *J. Chem. Soc., Dalton Trans.* **1996**, 255−270.
(6) Kawamura-Kuribayashi, H.; Koga, N.; Morokuma, K. *J. Am. Chem. Soc.* **1992**, *114*, 8687.
(7) Woo, T. K.; Fan, L.; Ziegler, T. *Organometallics* **1994**, *13*, 432−433.
(8) Fan, L.; Harrison, D.; Woo, T. K.; Ziegler, T. *Organometallics* **1995**, *14*, 2018−2026.
(9) Lohrenz, J. C. W.; Woo, T. K.; Ziegler, T. *J. Am. Chem. Soc.* **1995**, *117*, 12793−12800.
(10) Fusco, R.; Spera, S.; Longo, L.; Proto, A.; Abis, L.; Accomazzi, P.; Gila, L.; Guarini, A.; Bertoni, S.; Busetto, C.; Garbassi, F. In *Proceedings 2nd International Congress on Metallocene Polymers; Metallocenes 96*; Schotland Inc.: Skillman, NJ, 1996; pp 337−350.
(11) Cossee, P. *J. Catal.* **1963**, *3*, 80−88.
(12) Burger, B. J.; Thompson, M. E.; Cotter, W. D.; Bercaw, J. E. *J. Am. Chem. Soc.* **1990**, *112*, 1566−1577.
(13) Woo, T. K.; Fan, L.; Ziegler, T. *Organometallics* **1994**, *13*, 2252−2261.
(14) Yoshida, T.; Koga, N.; Morokuma, K. *Organometallics* **1994**, *14*, 746−758.
(15) Lohrenz, J. C. W.; Woo, T. K.; Fan. L.; Ziegler, T. *J. Organomet. Chem.* **1995**, *497*, 91−104.
(16) Cavallo, L.; Guerra, G. *Macromolecules* **1996**, *29*, 2729−2737.
(17) Støvneng, J. A.; Rytter, E. *J. Organomet. Chem.* **1996**, *519*, 277−280.
(18) Woo, T. K.; Margl, P. M.; Ziegler, T.; Blöchl, P. E. *Organometallics* **1997**, *16*, 3454−3468.
(19) Thorshaug, K.; Rytter, E.; Ystenes, M. *Macromol. Rapid Commun.* **1997**, *18*, 715−722.
(20) Chien, J. C. W.; Wang, B. P. *J. Polym. Sci., Part A: Polym. Chem.* **1990**, *28*, 15−38.
(21) Stehling, U; Diebold, J.; Kirsten, R.; Roll, W.; Brintzinger, H. H.; Jüngling, S.; Mülhaupt, R.; Langhauser, F. *Organometallics* **1994**, *13*, 964−970.
(22) Resconi, L.; Piemontesi, F.; Franciscono, G.; Abis, L.; Fiorani, T. *J. Am. Chem. Soc.* **1992**, *114*, 1025−1032.
(23) Mogstad, A. M.; Waymouth, R. M. *Macromolecules* **1992**, *25*, 2282−2284.
(24) Alelyunas, Y. W.; Guo, Z.; LaPointe, R. E.; Jordan, R. F. *Organometallics* **1993**, *12*, 544−553.
(25) D'Agnillo, L.; Soares, J. B. P.; Penlidis, A. *Macromol. Chem. Phys.*, in press.
(26) Busico, V; Cipullo, R. *J. Am. Chem. Soc.* **1994**, *116*, 9329−9330.
(27) Busico, V.; Caporaso, L.; Cipullo, R.; Landriani, L.; Angelini, G.; Margonelli, A.; Segre, A. L. *J. Am. Chem. Soc.* **1996**, *118*, 2105−2106.
(28) Busico, V.; Cipullo, R. *J. Organomet. Chem.* **1995**, *497*, 113−118.
(29) Busico, V.; Cipullo, R. In *Proceedings 2nd International Congress on Metallocene Polymers; Metallocenes 96*, Schotland Inc.: Skillman, NJ, 1996; pp 325−333.
(30) Leclerc, M. K.; Brintzinger, H. H. *J. Am. Chem. Soc.* **1995**, *117*, 1651−1652.
(31) Leclerc, M. K.; Brintzinger, H. H. *J. Am. Chem. Soc.* **1996**, *118*, 9024−9032.
(32) Prosenc, M. H.; Brintzinger, H. H. *Organometallics* **1997**, *16*, 3889−3894.
(33) Janiak, C.; Versteeg, U.; Lange, K. C. H.; Weimann, R.; Hahn, E. *J. Organomet. Chem.* **1995**, *501*, 219−234.
(34) Kaminsky, W.; Külper, K.; Niedoba, S. *Makromol. Chem., Macromol. Symp.* **1986**, *3*, 377−387.
(35) Ewen, J. A. In *Studies in Surface Science Catalysis;* Keii, T., Soga, K. Eds.; Kodansha Elsevier: Tokyo, 1986; Vol. 25, pp 271−292.
(36) DMol User Guide September 1996; Molecular Simulations: San Diego, 1996.
(37) Lee, C.; Yang, W.; Parr, R. G. *Phys. Rev. B* **1988**, *37*, 785−789.
(38) Becke, A. D. *Phys. Rev. A* **1988**, *38*, 3090−3100.
(39) The activation and reaction *energies* are slightly different from the corresponding *enthalpies*, in particular for a bimolecular addition reaction, where the difference amounts approximately to the difference in zero-point vibrational energy (ZPVE) between reactants and product. Since the number of vibrational degrees of freedom is larger for the single-product molecule than for the two reactant molecules, one expects an increase of the ZPVE in the addition reaction. Hence, reaction energies will typically be somewhat larger than reaction enthalpies. However, we expect only small differences in activation energies and corresponding enthalpies, since there is no particular reason for large differences in the ZPVE between the initial local energy minimum (for chain propagation, the π-complex) and the transition state of a given reaction. In fact, for the "model" reaction $Cp_2ZrCH_3^+ + C_2H_4 \rightarrow Cp_2ZrC_3H_7^+$ we find a reaction energy and zero-point reaction enthalpy of −80 and −57 kJ/mol, respectively, whereas the corresponding numbers for the insertion barrier are 26 and 33 kJ/mol. This agrees well with our expectations and leaves considerable justification for using

the calculated activation energies in a discussion of the experiments.
(40) Wester, T. S.; Johnsen, H.; Kittilsen, P.; Rytter, E. *Macromol. Chem. Phys.*, in press.
(41) Chien, J. C. W.; Wang, B. P. *J. Polym. Sci., Part A: Polym. Chem.* **1988**, *26*, 3089−3102.
(42) Mallin, D. T.; Rausch, M. D.; Chien, J. C. W. *Polym. Bull.* **1988**, *20*, 421−425.
(43) Peng, K.; Xiao, S. *J. Mol. Catal.* **1994**, *90*, 201−211.
(44) Eskelinen, M.; Seppälä, J. V. *Eur. Polym. J.* **1996**, *32*, 331−335.
(45) Froment, G. F.; Bischoff, K. B. *Chemical Reactor Analysis and Design*, 2nd ed.; Wiley: New York, 1990; p 167.
(46) In Figure 7A, we have omitted the data from runs 6 and 22 from the FTIR measurements and run 15 from the GPC measurement because these values clearly deviate more than 3 times the standard deviation of the data.
(47) Blom, R.; Dahl, I. M. *Macromol. Chem. Phys.*, in press.
(48) Jordan, R. F. *J. Chem Educ.* **1988**, *65*, 285−289.
(49) Eisch, J.; Caldwell, K.; Werner, S.; Kruger, C. *Organometallics* **1991**, *10*, 3417−3419.
(50) Some attempts to model the influence of MAO on the polymerization have appeared in the literature lately, see, e.g., ref 10 and: Fusco, R.; Longo, L.; Masi, F.; Garbassi, F. *Macromolecules* **1997**, *30*, 7673−7685.
(51) Darwent, B. D. B. *Bond Dissociation Energies in Simple Molecules*; NSRDS-NBS 31; GPO: Washington, DC, 1970.
(52) For the $\gamma \rightarrow \beta$ rotation reaction with L = Cp, the transition state has been formally optimized and verified to possess a single imaginary vibrational frequency of about 122 cm^{-1}.
(53) Some of the calculations with L = Cp were performed with a propyl chain, whereas with L = Cp*, we have always started with a butyl chain. With β-agostic structures, we have verified that there are only minor differences between results based on a propyl and a butyl chain. However, in connection with the isomerization reaction, it is necessary to use at least a butyl chain.
(54) Alternative LT coordinates for the $\pi_\beta \rightarrow \pi_\alpha$ reaction have been tried for the L = Cp catalyst, but the lowest energy barrier was found with the angle $Zr-C_\alpha-C_\beta$.
(55) Backside insertion into a γ-agostic structure has been attempted but found to be extremely unlikely. The activation energy is more than 170 kJ/mol, even with L = Cp.
(56) An attempt to model termination by transfer of a γ-hydrogen shows that it is highly unlikely. This is as expected, since it would have to be accompanied by additional hydrogen migration.
(57) Aylward, G. H.; Findlay, T. J. V. *SI chemical data*, 2nd ed.; Wiley: Australia, 1974.

MA980694K